

THEORIES OF FRONTOGENESIS

Prof. Huw C. Davies

Institute for Atmospheric and Climate Science

Author's Address:

Prof. Huw C. Davies,
Institute for Atmospheric and Climate Science
Universitätsstrasse 16
ETH Zentrum, CHN
8092 Zürich
Switzerland
e-mail: huw.davies@env.ethz.ch

Abstract

A review is presented of theoretical frontogenesis studies. The framework for the study is that of quasi- and semi-geostrophic dynamics, and the approach is to consider idealized models that incorporate some presumed quintessential frontogenetic process(es). The focus of the study is the temporal development and nature of surface fronts.

Insight is sought first from consideration of two archetypal settings for two-dimensional frontal formation - the Bergeron configuration for deformation-induced frontogenesis and the Eliassen configuration for horizontal shear-induced frontogenesis. These two settings serve to illustrate the role of the ageostrophic circulation in frontal scale-contraction and the key features and distinction between prototype cold and warm fronts. They also form a platform for the exploration of the factors that can limit the scale-contraction and generate unbalanced flow, and the examination of frictional and diabatic effects.

The concurrent development of fronts and cyclones is studied in the extended Eady-setting of baroclinic waves growing on a jet-like basic flow. Simulations reproduce variants of the classic X-shaped configuration for the surface frontal palette that include elongated cold fronts, warm fronts that arch around the centre of the depression, and the fracture of the cold front in the vicinity of the cyclone. Consideration is also given to the frontal palette associated with paradigmatic precursor patterns for cyclogenesis. Diagnostic analyses based predominantly on the potential vorticity perspective illuminate the role of ambient lateral shear and the precursor flow pattern in determining the nature of the frontal palette.

Chapter 1

Introduction

Fronts in the form of elongated (1000 km long and 100 km wide) bands of enhanced baroclinicity are distinctive and key features of surface weather patterns. The terms frontogenesis and frontolysis were introduced to signify respectively the dynamical development and decay of such fronts and were coined by a member of the Bergen School (Bergeron, 1928). There were three salient ingredients to Bergeron's landmark study. First there was the recognition that fronts were not immutable but underwent a life-cycle. Thus the study directed attention to the role of the larger-scale flow in generating fronts and was a counterpoint to the Bergen School's earlier portrayal of mid-latitude weather patterns in terms of the distortion and convolution of the pre-existing polar-front. Secondly there was the identification and the theoretical consideration of the possible frontogenetic role of deformation in frontogenesis. His study constitutes a forerunner of a class of theoretical frontogenesis studies that, based upon idealized and readily analyzable mathematical models that incorporate some presumed quintessential frontogenetic feature(s), seek to advance our understanding insight of the natural phenomena. Thirdly Bergeron explored briefly the implications of the linkage between deformation and frontogenesis to the climatology of surface fronts.

This review attempts to follow the same pattern. It seeks to distil the knowledge and understanding of frontal dynamics that has been gained from idealized mathematical models, and to relate the results to the observed range of fronts. Particular consideration will be given to the factors that determine the temporal development, nature, and classification of surface fronts.

Chapter 2

Observational and theoretical backcloth

2.1 Some Salient Observational Characteristics

Surface fronts are regarded as slender transition zones possessing certain salient flow characteristics. These include the forementioned enhancement of the horizontal baroclinicity ($\nabla_h \theta$) relative to the background value, a cyclonic wind shift and a kink in the isobars across the zone - consistent with the existence of a locally intensified vertical component of relative vorticity (ζ), significant pre-frontal bands of strong relative airflow (so-called frontal air-streams), and substantial bands of convergence and cloud activity. Cold fronts are usually elongated and often match this standard description whereas warm fronts tend to be stubbier, less distinct at the surface, and with a shallower slope aloft.

Both cold and warm fronts are depicted on surface synoptic charts as either the main components of an incipient wave disturbance growing within a frontal zone or, in combination with their occluded progeny, as the sub-synoptic embroidery of a maturing or matured low pressure system. An incipient frontal palette accompanying cyclogenesis exhibits a \wedge shape in the Northern Hemisphere with the apex at the cyclones centre and the SW and SE directed segments corresponding to the cold and warm fronts. Thereafter the pattern frequently evolves to λ -shape with the cold front appearing to overtake the warm front to form an "occlusion" in the neighbourhood of the cyclone. However there is considerable variation from event to event, and particularly noteworthy are the following variants:- the frequent absence of a distinct warm frontal structure with merely the presence of an amorphous band of "weather" in its presumed vicinity; the non-occurrence of an occlusion process; a fracture of the original baroclinic zone such that the cold front is dislocated from the cyclone; and the occurrence of a strong warm front that arches around the poleward sector of the Low.

There are also strong regional differences in the form of the prevalent frontal types. For example synoptic experience suggests that warm fronts tend to occur less frequently in the vicinity of Australia, whereas they are the most frequent and distinctive frontal type over north-eastern Canada.

2.2 A Theoretical Framework

First consider the theoretical rudiments of frontogenesis. A natural starting point is to examine the kinematics accompanying the generation of intense thermal gradients. Vector and scalar forms for the Lagrangian development of a fluid parcel's potential temperature gradient ($\nabla\theta$) are,

$$\frac{D}{Dt}(\nabla\theta) = -(\nabla\theta \cdot \nabla)\mathbf{v} - (\nabla\theta \times \boldsymbol{\omega}) + \nabla E, \quad (2.1)$$

and

$$\begin{aligned} \frac{D}{Dt} \frac{1}{2}(\nabla\theta)^2 &= -(\nabla\theta) \cdot (\nabla\theta \cdot \nabla)\mathbf{v} + (\nabla\theta) \cdot (\nabla E) \\ &= -(\nabla\theta)^2 \left(\frac{\partial\nu}{\partial n} \right) + (\nabla\theta) \cdot (\nabla E) \end{aligned} \quad (2.2)$$

Here $\boldsymbol{\omega}$ is the vector vorticity, E is a term proportional to the diabatic heating rate, and ν is the velocity component in the n -direction aligned perpendicular to the isentropes along the baroclinicity vector. (Lalaurette et al, 1994 record the tensor equivalent of the foregoing relationships).

Eq. 2.1 indicates that, following a fluid parcel, the three-dimensional baroclinicity ($\nabla\theta$) can be modified in three ways : - a tendency for "baroclinicity lines" to move *against* the flow (c.f. the equation for a material line $Da/Dt = (a \cdot \nabla)\mathbf{v}$ involving both tilting and compression; reorientation by the ambient vorticity; and generation / destruction due to spatial variations of diabatic effects. Likewise Eq. 2.2 emphasizes that a decrease of ν along the baroclinicity vector connotes frontogenesis.

There are three significant caveats attached to the foregoing general formulae. Firstly surface frontogenesis is usually linked to the horizontal component ($\nabla_h\theta$) of the baroclinicity. Hence it is appropriate to note that at flat surface the adiabatic form of Eq. 2.2 reduces to (Petterssen, 1936),

$$\frac{D}{Dt} \|\nabla_h\theta\| = \frac{1}{2} \|\nabla_h\theta\| \{D \cos(2\delta) - (\nabla \cdot v_h)\} \quad (2.3)$$

where D is the resultant deformation and δ is the local angle between the dilatation axis and the surface isentrope. This vector invariant form of the equation serves to emphasize the role of deformation and horizontal divergence, and moreover the latter term disappears in the geostrophic limit.

Secondly in a framework moving with the front, the along-front wind component tends to dominate the across-front component. This hampers direct inference of the frontogenetic tendency using Eq. 2.2, since this involves estimating the spatial gradient ($\partial\nu/\partial n$) of the across-front flow. In the geostrophic limit this difficulty can be circumvented since at the surface the equivalent of Eq. 2.1 takes the form (Hoskins et al. 1978),

$$\begin{aligned} \frac{D}{Dt} (\nabla_h\theta) &= Q + \nabla_h E \\ \text{where } Q &= -\|\nabla_h\theta\| \left\{ k \times \left(\frac{\partial \mathbf{v}_g}{\partial s} \right) \right\} \end{aligned} \quad (2.4)$$

with (s, n) prescribing a local cartesian framework such that s is aligned along an isentrope and n points toward low thermal values. Thus in this formulation the frontogenetic forcing \mathbf{Q} is expressed in terms of the product of $(\nabla_h\theta)$ and the along-front variation of the geostrophic velocity (\mathbf{v}_g), and an useful qualitative appraisal of the frontogenetic tendency can be ascertained directly by a visual inspection of the geopotential and thermal fields on a standard low-level synoptic chart. The vector \mathbf{Q} can also be recast in natural coordinates (Keyser et.al, 1988) or decomposed into its invariant components (Schär and Wernli, 1993).

The third caveat pertains to all the foregoing formulae. Each provides a kinematic index of the frontogenesis experienced by fluid parcels that are within but also possibly traversing across a frontal zone, as opposed to representing a dynamic frontogenesis index for the front itself.

Consideration of frontal dynamics requires an internally consistent, self-contained and appropriate theoretical framework. The focus here is on the quintessence of frontogenesis and this can be explored using the quasi-geostrophic set of equations (QG) for an incompressible and inviscid fluid on an f-plane. The set takes the compact form expressed by the conservation, in the absence of diabolic effects, of quasi-geostrophic potential vorticity (q) in the interior,

$$\frac{D}{Dt_{QG}}(q) = \frac{f}{N^2} \frac{g}{\theta_0} \frac{\partial E}{\partial z}, \quad (2.5a)$$

and potential temperature at rigid horizontal boundaries,

$$\frac{D}{Dt}\theta = E \quad \text{at say} \quad z = 0 \quad (2.5b)$$

$$\text{where } \frac{D}{Dt_{QG}} = \{\partial/\partial t + u_g\partial/\partial x + v_g\partial/\partial y\} \quad (2.5c)$$

is the advective derivative following the geostrophic flow $\mathbf{v}_g[-\partial\Psi/\partial y, \partial\Psi/\partial x]$. The potential vorticity (q) is given by,

$$q = \{\nabla_h^2\Psi + (f/N)^2\partial^2\Psi/\partial z^2\} \quad (2.5d)$$

and here the potential temperature (θ)

$$\frac{g}{\theta_0}\theta = f \left(\frac{\partial\Psi}{\partial z} \right) \quad (2.5e)$$

refers to the deviation from a basic state defined by a reference value θ_0 . plus an ambient stratification N^2 (here assumed for simplicity to be uniform). In this framework key frontal parameters - the vertical component of vorticity (ζ), the vertical velocity (w), and the baroclinicity ($\nabla_h\theta$) at the surface - are inter-related via the equations,

$$\frac{D}{Dt_{QG}}(\zeta) = f \frac{\partial w}{\partial z} \quad (2.5)$$

$$N^2(\nabla_h^2 w) + f^2 \frac{\partial^2 w}{\partial z^2} = \frac{g}{\theta_0}(2\nabla_h Q + \nabla_h^2 E) \quad (2.6)$$

$$\frac{D}{Dt_{QG}}(\nabla_h\theta) = \mathbf{Q}\nabla_h(E) \quad \text{at } z = 0 \quad (2.7)$$

Hence a suitable distribution of ageostrophic forcing (i.e. the \mathbf{Q} field) and/or diabatic heating (- the E -field) within a frontal zone could concomitantly enhance the ambient thermal gradient Eq. 2.8, induce low-level ascent Eq. 2.7, and thereby increase the vorticity Eq. 2.6. The basic QG set Eqs. 2.5 is itself internally consistent and self-contained provided the diabatic heating rate is expressible in terms of the geostrophic field. However in the present context the appropriateness of the set is called into question by the intrinsic sub-synoptic space and time scales of observed frontogenesis events. Major shortcomings are linked to the strength of the ageostrophic circulation (and with it the neglect of tilting effects in Eq. 2.8), the amplitude of the relative vorticity (ζ), and the horizontal variation of the stratification. The ageostrophic circulation can be significant and, although partially prescribed by Eq. 2.7, it is not taken into account in the advection of q and θ (Eq. 2.5 a-b). Likewise ζ attains values comparable to f , but $(\zeta + f)$ is

replaced by f in the term (on the right hand side of Eq. 2.6) for the production of vorticity due to horizontal convergence.

These shortcomings are to a measure circumvented in the semi-geostrophic system (SG). It is based on the observation that frontal flow is quasi-balanced with anisotropic synoptic along-front and meso across-front scales, and that on a time-scale comparable to f^{-1} the fluid parcels move predominantly along rather than traversing substantially across the frontal zone. The resulting inference is that the essence of two-dimensional frontogenesis is captured by assuming geostrophy of the along-front flow component, i.e. the semi-geostrophic approximation (Eliassen, 1962). A natural extension to three-dimensions is the so-called geostrophic momentum system (Hoskins, 1975) wherein the geostrophic momentum is advected by the sum of the two-dimensional geostrophic flow (\mathbf{v}_g) and the three-dimensional geostrophically-forced ageostrophic flow (\mathbf{v}_{ag}), i.e.

$$\frac{D}{Dt_{SG}}(\mathbf{v}_g) = \left[\frac{\partial}{\partial t} + (\mathbf{v}_g + \mathbf{v}_{ag}) \cdot \nabla \right] \mathbf{v}_g \quad (2.8)$$

Here and hereafter the terms semi-geostrophic and geostrophic momentum are deemed synonymous. Hoskins (1975) further showed that, subject to the transform,

$$[X, Y, Z, T] = \left[x + \frac{v_g}{f}, y - \frac{u_g}{f}, z, t \right] \quad (2.9)$$

the SG set assumes a form similar to that of the QG set, and indeed the two are isomorphic for the case of uniform interior potential vorticity. The philosophy adopted here is to seek insight and qualitative interpretations using the the QG and SG sets but bearing in mind their limitations.

Chapter 3

Frontogenesis in two-dimensions

Quasi two-dimensional models of frontogenesis are idealizations geared specifically to elucidating the nature of the process in the presence of certain simple archetypal \mathbf{Q} -Field configurations. Two basic configurations for frontogenesis (assumed to be aligned along the y -coordinate) are illustrated in Fig. 3.1, and they represent : - (a) a horizontal deformation field, $[u_d = -\alpha x, v_d = \alpha y]$, acting on a two-dimensional thermal distribution $\theta = \theta(x, z)$; and (b) horizontal shear $v = v(x, z)$ aligned transverse to an ambient field of uniform baroclinicity $U = \Lambda z$. These

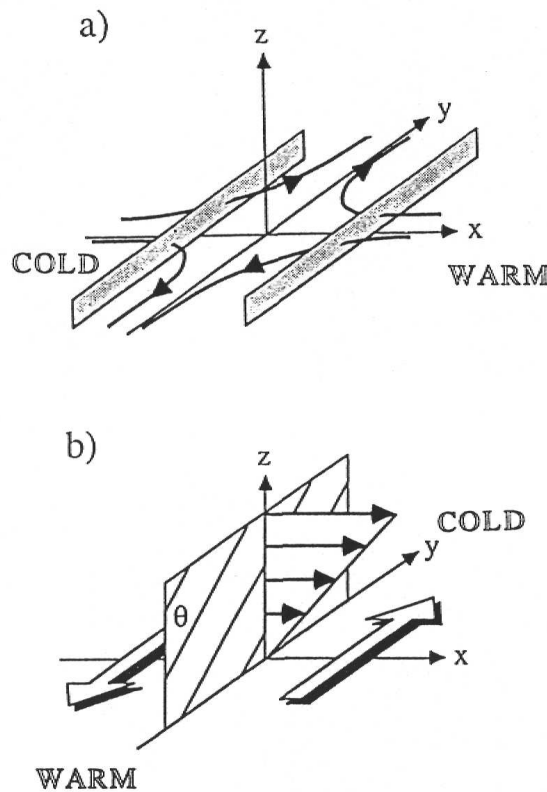


Figure 3.1: Schematic of the basic states for (a) the Bergeron and (b) the Eliassen archetypal settings corresponding respectively to deformation-induced and horizontal shear-induced frontogenesis.

two configurations correspond respectively to those postulated by Bergeron (1928) and Eliassen (1959, 1990). At the surface they represent the two forcing terms in the x-component of Eq. 2.1, i.e.

$$\frac{D}{Dt} \left(\frac{\partial \theta}{\partial x} \right) = - \left(\frac{\partial \theta}{\partial x} \frac{\partial u}{\partial x} + \frac{\partial \theta}{\partial y} \frac{\partial v}{\partial x} \right) \quad \text{at } z = 0 \quad (3.1)$$

The time development of these two configurations has been the subject of intensive study for the limit-case of the *adiabatic* and *inviscid* flow of a medium of *uniform* potential vorticity (e.g. Stone, 1966; Williams, 1967, 1968; Hoskins, 1971; Hoskins and Bretherton, 1972; Blumen, 1981; Bannon, 1984; Davies and Muller, 1988).

In this limit the SG set take the form of Eqs. 2.5 with (x, z, t) replaced by (X, Z, T) , so that the equation for the potential vorticity departure away from its uniform background value is

$$\Psi_{xx} + \left(\frac{N}{f} \right)^2 \Psi_{zz} = 0, \quad (3.2)$$

and the thermal boundary equation is a reduced form of Eq. 2.5b. Also the cross-front ageostrophic circulation can be deduced from the Sawyer-Eliassen Equation (Sawyer, 1956; Eliassen, 1962) for the stream-function (χ),

$$\left(\frac{N}{f} \right)^2 \chi_{xx} + \chi_{zz} = \mathcal{F} \quad (3.3)$$

This is a two-dimensional refined form of Eq. 2.8 with \mathcal{F} denoting the geostrophic forcing field and the ageostrophic flow components given by $(u', w) = [-(\partial\chi/\partial z), (\partial\chi/\partial x)]$. Specific solutions of this system (i.e. Eqs. 3.2, 2.5b, and 3.3) can be derived in geostrophic space, $[X, Z, T]$, and then displayed in physical space using the reverse of the transform (2.10). The approach adopted here is to first consider separately surface frontogenesis for the two foregoing configurations, and then to comment upon their limitations and the modifying effect of cloud diabatic heating and surface friction.

3.1 Deformation-induced Frontogenesis

For illustrative purposes consider a semi-infinite domain ($z > 0$) with a flow setting comprising a pure horizontal deformation field, $(u_d = -\alpha x, v_d = \alpha y)$, and an initial thermal distribution composed of a reference potential temperature θ_0 , uniform stratification N , and a spatial variation $\theta = \theta(X, Z)$.

Surface frontogenesis accomplished by the deformation field alone - i.e. merely by the quasi-geostrophic flow (or equivalently by the dynamics in geostrophic space) - is described by the following reduced form of Eq. 3.1,

$$\frac{D}{Dt_{SG}} \left(\frac{\partial \theta}{\partial X} \right) = \alpha \frac{\partial \theta}{\partial X} \quad \text{at } Z = 0$$

Hence at the surface a fluid parcel's baroclinicity would increase such that after a lapse-time T ,

$$\left(\frac{\partial \theta}{\partial X} \right)_{T=T} = \left(\frac{\partial \theta}{\partial X} \right)_{T=0} \exp(\alpha T),$$

and it would require an infinite time to develop a frontal discontinuity. The essence of the SG dynamics can be inferred as follows. For this configuration the geostrophic forcing field \mathcal{F}

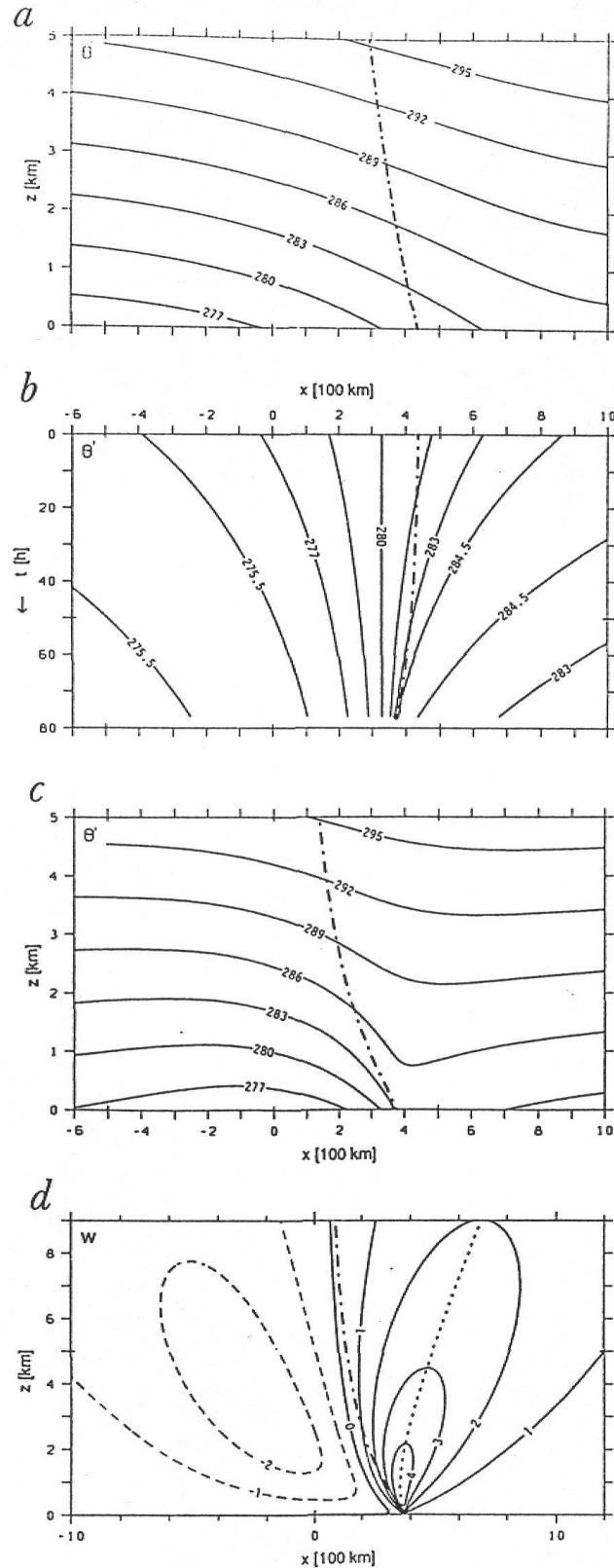


Figure 3.2: Features of a semi-geostrophic realization of deformation-induced frontogenesis. The panels show:- (a) the cross-section of the initial isentropic distribution, (b) the space-time development of the surface isentropes, and (c and d) depict respectively the cross-sectional distribution of the isentropic distribution and the vertical velocity field shortly before frontal collapse. The dash-dot curves refer to the baroclinicity maximum, and the dotted line in panel d demarks the vorticity maximum. Units are degrees K for the isentropes and $mm\ s^{-1}$ for the vertical velocity. (Adapted from Davies and Müller, 1988).

takes the form,

$$\begin{aligned}\mathcal{F} &= +2\frac{\alpha}{f^2}\frac{g}{\theta_0}\frac{\partial\theta}{\partial X} \\ &= +2\frac{\alpha}{f}\frac{\partial v}{\partial Z}\end{aligned}$$

The solution of Eq. 3.3 in the half space $Z > 0$ is given (Davies and Muller, 1988) by,

$$\begin{aligned}\chi &= \frac{\alpha}{f}zv + \text{const} \\ \text{so that, } u' &= -\frac{\alpha}{f}\left(v + z\frac{\partial v}{\partial z}\right), \text{ and } w = \frac{\alpha}{f}\left(v + z\frac{\partial v}{\partial x}\right),\end{aligned}\quad (3.4)$$

It follows that at the surface,

$$\frac{\partial u'}{\partial x} = -\frac{\alpha}{f}\frac{\partial v}{\partial x}\quad (3.4b)$$

Hence the surface relative vorticity component $(\partial v/\partial x)$ and surface horizontal baroclinicity $(\partial\theta/\partial x)$ satisfy the equations (see Eqs. 2.9, and 3.1),

$$\frac{D}{Dt}_{SG}\left(\frac{\partial v}{\partial x}\right) = \frac{\alpha}{f}\frac{\partial v}{\partial x}\left(\frac{\partial v}{\partial x} + f\right), \quad \text{at } Z = 0\quad (3.5)$$

$$\frac{D}{Dt}_{SG}\left(\frac{\partial\theta}{\partial x}\right) = \frac{\alpha}{f}\frac{\partial\theta}{\partial x}\left(\frac{\partial v}{\partial x} + f\right), \quad \text{at } Z = 0\quad (3.6)$$

$$\frac{D}{Dt}_{SG}\left(\frac{\partial v}{\partial x}\frac{\partial\theta}{\partial x}\right) = 0 \quad \text{at } Z = 0\quad (3.7)$$

It follows, since the ageostrophic surface convergence remains in-phase with the surface vorticity (Eq. 3.4b), that the nonlinear vortex-stretching effect (the term on the right hand side of Eq. 3.5) and Q -forcing (the term on the right hand side of Eq. 3.6) continually increase the growth rates of the vorticity and baroclinicity of all surface fluid parcels with positive vorticity. Thus there is a sustained and increasing rate of frontogenesis, and the two frontal parameters become discontinuous after a lapse time t_c ,

$$\alpha t_c = \ln \left[1 + \left(\frac{f}{v_x} \right)_{\max(z=0, t=0)} \right]\quad (3.8)$$

An example of deformation-induced frontogenesis is displayed in Fig 3.2. It shows in physical space the solution whose thermal development in geostrophic space (X, Z, T) is given by,

$$\theta(X, Z, T) = \frac{\Delta\theta X^*}{(X^*)^2 + (Z^*)^2} \quad \text{for } Z > 0,\quad (3.9)$$

where $X^* = (X/L)\exp(\alpha T)$ and $Z^* = [1 + (N/f)^2(Z/L)\exp(\alpha T)]$ In effect an initial thermal transition zone of amplitude $\Delta\theta$ and width $2L$ (see Fig. 3.2a) undergoes a scale contraction (Fig. 3.2b) and attains an infinite value of surface baroclinicity (and vorticity) after a time $t = t_c$,

$$\alpha t_c = \ln \left[\frac{8}{3\sqrt{3}} R_o^{-1} \right]\quad (3.10)$$

at the location $x = x_c$,

$$\frac{x_c}{L} = \frac{9}{8}R_o \left[1 + \frac{\Xi}{\sqrt{3}}L \right] \quad (3.11)$$

Here $R_o = V/(fL)$ is a Rossby Number based upon a measure (V) of the along-front velocity, $V = [g(\Delta\Theta)/(N\theta_0)]$, and Ξ refers to an initial displacement of the θ -field relative to the dilatation axis. In the approach to this scale collapse the vertical slope of the baroclinicity maximum (see Fig. 3.2c) can be shown to approach the value $\sim \sqrt{3}(f/N)$. The direct ageostrophic circulation, with surface convergence focused at the vorticity maximum and ascent aligned along this baroclinicity axis, is evident in Fig. 3.2d.

The development is governed by the two dimensionless parameters - R_o and (Ξ/L) . Higher values of R_o - i.e. stronger fronts and/or a less stable ambient atmosphere (c.f. Bannon, 1984) - induce a more rapid frontogenesis. For typical atmospheric values $t_c \sim 3$ days. This is not particularly rapid since it is comparable to the time scale of cyclogenesis and moreover our idealised model assumes that the deformation remains optimally aligned to the baroclinicity throughout the frontal contraction. Again the relative displacement (Ξ/L) modifies the propagation speed and the final location x_c of the baroclinicity maximum, but not the internal frontal structure. Hence the direction of frontal movement, determined by the sign of the factor $[1 + \Xi/\sqrt{3}L]$ - see Eq. 3.1, is not a dynamical indicator of the strength (strong/weak) or type (cold/warm) of the front.

Ancillary inferences can also be drawn from Eq. 3.5 regarding frontal predictability and the development of multiple fronts. Firstly from Eq. 3.5 it can be deduced that errors in the vorticity field will amplify rapidly (decay) in regions of positive (negative) relative vorticity. In turn this implies that for this idealized model setting accurate prediction of frontogenesis requires an accurate specification of the flow field within and in the vicinity of the frontal zone. Secondly a surface vorticity maximum is always linked to the same fluid parcel, and each local maximum will undergo frontogenesis. Thus the presence of vorticity / thermal maxima within the zone will lead to a multiple frontal structure, and this bolsters the suggestion (Hoskins et al. 1984) that frontal rainbands may be caused by mesoscale inhomogeneities in the surface temperature field.

It is apparent from the foregoing that frontogenesis induced by a pure deformation field, although clearly an overt idealization of the observed phenomenon, serves as an excellent theoretical model in so far that it readily yields a rich variety of transparent and conceptual insights. There are also occasions when it replicates the evolution of an observed event (see e.g. Ostdiek and Blumen, 1995). However the amplitude ($\sim 1 \text{ cm s}^{-1}$) of the vertical velocity induced in this setting is significantly less than that of observed frontal ascent and this suggests that other effects, in particular diabatic and surface frictional effects, are seminal to this aspect of frontogenesis.

3.2 Horizontal Shear-induced Frontogenesis

In this configuration a horizontal shear $v = v(x, z)$ is aligned transverse to an ambient field of uniform baroclinicity with its associated shear, $U = \Lambda z$. The rate of surface frontogenesis is now prescribed by the other reduced form of Eq. 3.1,

$$\text{viz. } \frac{D}{Dt} \left(\frac{\partial\theta}{\partial x} \right) = - \left[\left(\frac{\partial\theta}{\partial y} \right) \left(\frac{\partial v}{\partial x} \right) \right] \quad \text{at } z = 0 \quad (3.12)$$

i.e. the baroclinicity of a fluid parcel will increase if the vorticity and baroclinicity are suitably correlated. In the SG limit the equations governing this system are: the expression for

the PV (i.e. Eq. 3.2),

$$\left[\Psi_{xx} + \left(\frac{f}{N} \right)^2 \Psi_{zz} \right] = 0 \quad (3.13)$$

and the thermal development on the bounding surface(s) - the reduced form of Eq. (2.5b),

$$\text{i.e. } \left[\frac{\partial}{\partial T} + u \frac{\partial}{\partial X} \right] \left(\frac{g}{\theta_0} \right) (\theta) - (\Lambda f)v = 0 \quad \text{at } Z = 0 \quad (3.14)$$

Also the forcing term in the Sawyer-Eliassen Equation (Eq. 3.3) now takes the form,

$$\mathcal{F} = -2 \frac{\Lambda}{N^2} \frac{g}{\theta_0} \frac{\partial \theta}{\partial Z} \quad (3.15)$$

Consider in turn frontogenesis in (I) vertically semi-infinite and (II) doubly-bounded domains. For Case (I) the dynamics of the linear flow system (Eqs. 3.13-3.14) in the semi-infinite domain ($Z > 0$) can be viewed as a composite of non-interacting surface thermal waves each of the form,

$$\begin{aligned} \theta(X, Z) &= B \sin(kX - \omega T) \exp[-(\mu z)] \\ \text{with } \omega &= \frac{\Lambda f}{N}, \quad \text{and} \quad \mu = \frac{Nk}{f} \end{aligned} \quad (3.16)$$

i.e. vertically-evanescent waves of constant amplitude (B) that propagate along the surface ($Z = 0$) in the positive x-direction with a phase-speed inversely proportional to their wavenumber (k). The corresponding group velocity is identically zero, and thus a packet of such waves will undergo a periodic temporal evolution with a period $T = 2\pi(N/\Lambda f)$, ~ 60 hours. Transient frontogenesis and frontolysis can occur as the baroclinicity of the individual waves experience constructive and destructive interference (Müller et al. 1989), and the accompanying ageostrophic circulation is given by the solution (see Müller et al. 1989) of Sawyer-Eliassen equation (Eq. 3.15),

$$\text{viz.} \quad \chi = - \left(\frac{\Lambda}{N^2} \right) \left(\frac{g}{\theta_0} \right) z\theta$$

Fig. 3.3 shows an example of such a cycle. A surface band of cold air is first replaced by a warm band advected from the south, and thereafter it is restored after the flow direction reverses (Fig.3.3a,b). Frontal features evolve rapidly on the western edge of the thermal anomalies and attain maturity at $(T/4)$ and $(3T/4)$. The cross-sectional structure at $(T/4)$ reveals features (see Fig. 3.3d-f) that bear comparison with typical warm fronts - a frontal region with a slope $\sim (f/N)$, a cold conveyor belt (Bjerknes, 1919; Browning, 1990) ahead of a comparatively weak surface front, and ascent through the frontal zone (c.f. Eliassen, 1962; Keyser and Pecnick, 1987).

Case (II), the bounded domain with rigid horizontal boundaries at say $Z = 0$ and d , is the Eady paradigm for baroclinic instability. For this case it is customary to examine the finite-time development of wave-like perturbations, and by analogy with Eq. 3.16 the system's dynamics in SG space comprise the interaction of two edge waves of the form (Davies and Bishop, 1994),

$$\theta_B = B(\sinh \mu d)^{-1} \{ \sinh[\mu(d - Z)] \} \sin(kX + \epsilon_B), \quad (3.17)$$

$$\theta_T = T(\sinh(\mu d))^{-1} \{ \sinh[(\mu Z)] \} \sin(kX + \epsilon_T), \quad (3.17b)$$

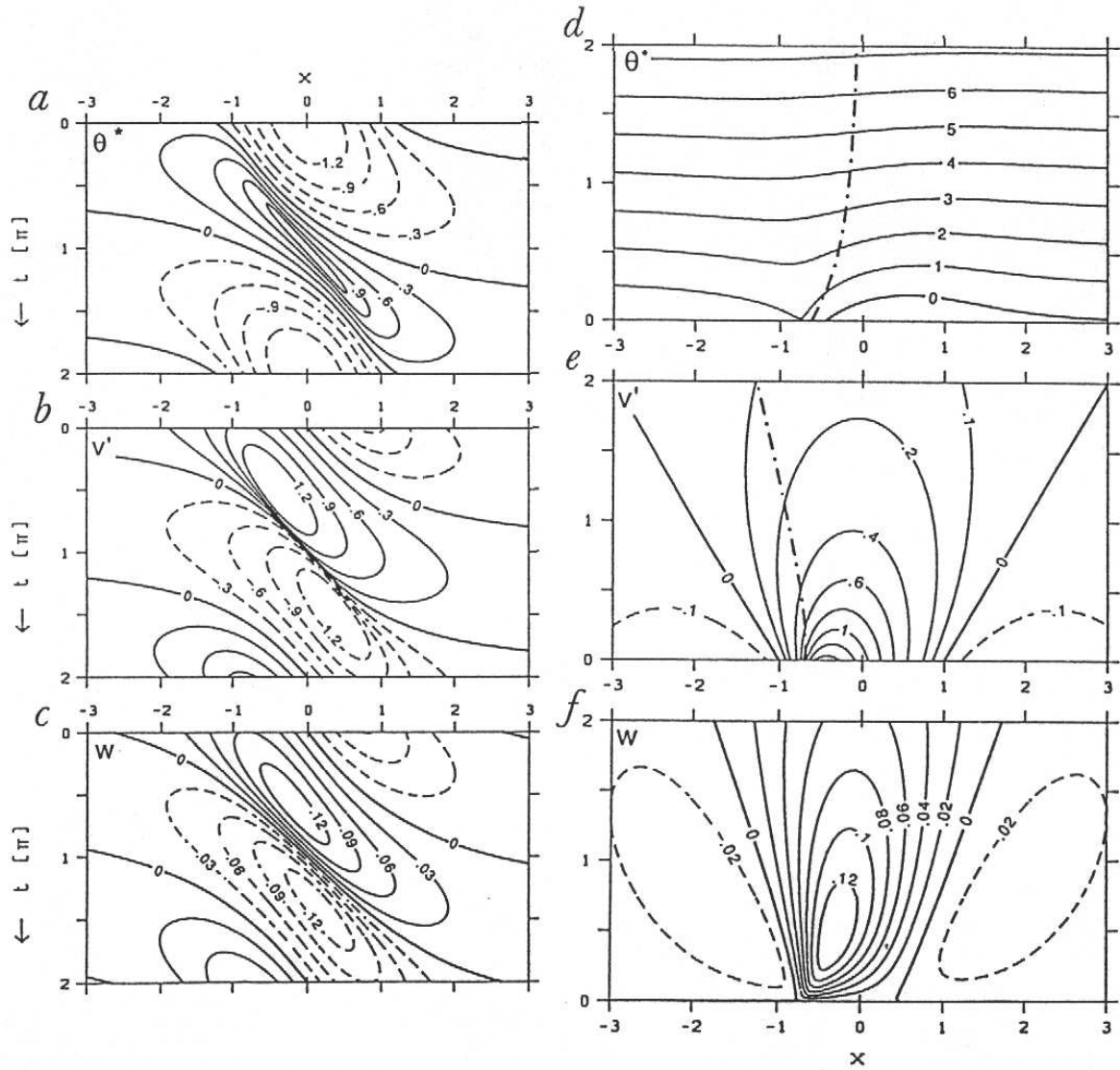


Figure 3.3: Features of a semi-geostrophic realization of a horizontal shear-induced frontogenesis in a semi-infinite domain. Left hand panels show the space-time development of (a) the isentropes and (b) the along-front wind component at the surface, and (c) the vertical wind field at height of 2.5 km. Panels (d, e, f) depict the cross-sectional distribution of the corresponding variables after a quarter of the cycle. The dash-dot curves refer to the baroclinicity maximum, and the parameter settings are such that unit values of (θ, v, w) correspond respectively to (20 K, 20ms^{-1} , and 0.15ms^{-1}). The domain of the cross-section is $(3000 * 10)\text{ km}$. (Adapted from Müller et.al. 1989)

with $\mu = (N/f)k$, the variables (B, ϵ_B) denoting respectively the time dependent amplitude and phase of the lower boundary wave, and (T, ϵ_T) representing the corresponding variables for the upper boundary wave. The temporal development is governed the time-scale $r = (\Lambda f/N)$ and a geometric factor $\alpha = [\cosh(\mu d) - (\mu d/2) \sinh(\mu d)]$.

From a PV perspective a warm anomaly at the lower (upper) boundary constitutes a positive (negative) PV anomaly with a δ -function vertical structure. The interaction of the two pseudo-PV surface waves arises from the advection of one boundary wave by the component of the flow field attributable to the other. This interaction can (i) enhance the wave-amplitude provided the relative phase, $\epsilon = (\epsilon_T - \epsilon_B)$, is negative (i.e. a westward slope to the pseudo-PV wave anomalies from the lower to the upper boundary), and (ii) counter the tendency of each wave to propagate against the ambient flow at its level. Synchronized development (i.e. $T = B$) will prevail if the waves are initially of equal amplitude, and for such a development the long wavelength waves (corresponding to $[1 - \alpha^2] > 0$) will amplify and evolve to a phase-locked state ($\epsilon = \text{const.}$). The special case with *ab initio* phase-locking corresponds to the exponentially growing Eady normal modes with a growth rate (σ_E),

$$\sigma_E = r \left[\frac{f}{N} k \operatorname{cosech}(\mu d) \right] (1 - \alpha^2)^{1/2}, \quad \text{with } \cos(\epsilon) = \alpha$$

The ageostrophic circulation distorts these waves and leads to a scale-collapse at the boundaries after a time t_c (Blumen, 1981) given by,

$$(\sigma_E t_c) = \ln \left(1 + \left(\frac{f}{v_x} \right)_{\max_{t=0}} \right)$$

Fig. (3.4a) shows the thermal structure of such a system in physical space immediately prior to the scale-collapse. It is reminiscent of a surface cold front maturing observed events include those of Blumen (1980), Ogura and Portis (1982) and Reeder and Smith (1986). The caveat regarding the weakness of the vertical velocity field applies in this case again, but nevertheless the degree of similitude with the observed events is surprising considering the overt simplicity of the model.

Alternative initial alignments of the pseudo-PV anomalies on the bounding surfaces, e.g. the two examples schematized in Figs. (3.4c, d), result in notably different flow evolutions. Consideration of the far-field contribution of the anomalies and their advection by the background shear suggests rapid cyclo- and fronto-genesis for the configuration of Fig. 3.4c as it transits toward the phase slope of growing Eady modes. In contrast incipient frontolysis can be expected for the case of Fig. 3.4d. These two cases bear comparison with, and shed light on, the differing form of evolution associated with the so-called cold and warm advection cases studied by Keyser and Pecnick (1987).

3.3 Other Two-dimensional Settings

A natural extension of the foregoing is to consider the combined effect of deformation and horizontal shear in inducing frontogenesis (Keyser and Pecnick, 1987). Bishop (1993) derived analytical solutions for this generalized setting in the limit of uniform potential vorticity. His results indicate that the presence of deformation orientated so as to increase the baroclinicity modifies the Eady-type instability such that smaller scale waves can evolve to form fronts.

Another setting for shear-induced frontogenesis is that of an uniformly sheared flow in a semi-infinite domain with an isolated interior PV anomaly (Thorncroft and Hoskins, 1990; Davies and Bishop, 1994). In the linear limit the interior anomaly is merely advected with the background flow at its level whilst continually forcing surface pseudo-PV / thermal waves (c.f. Eq. 3.16). For

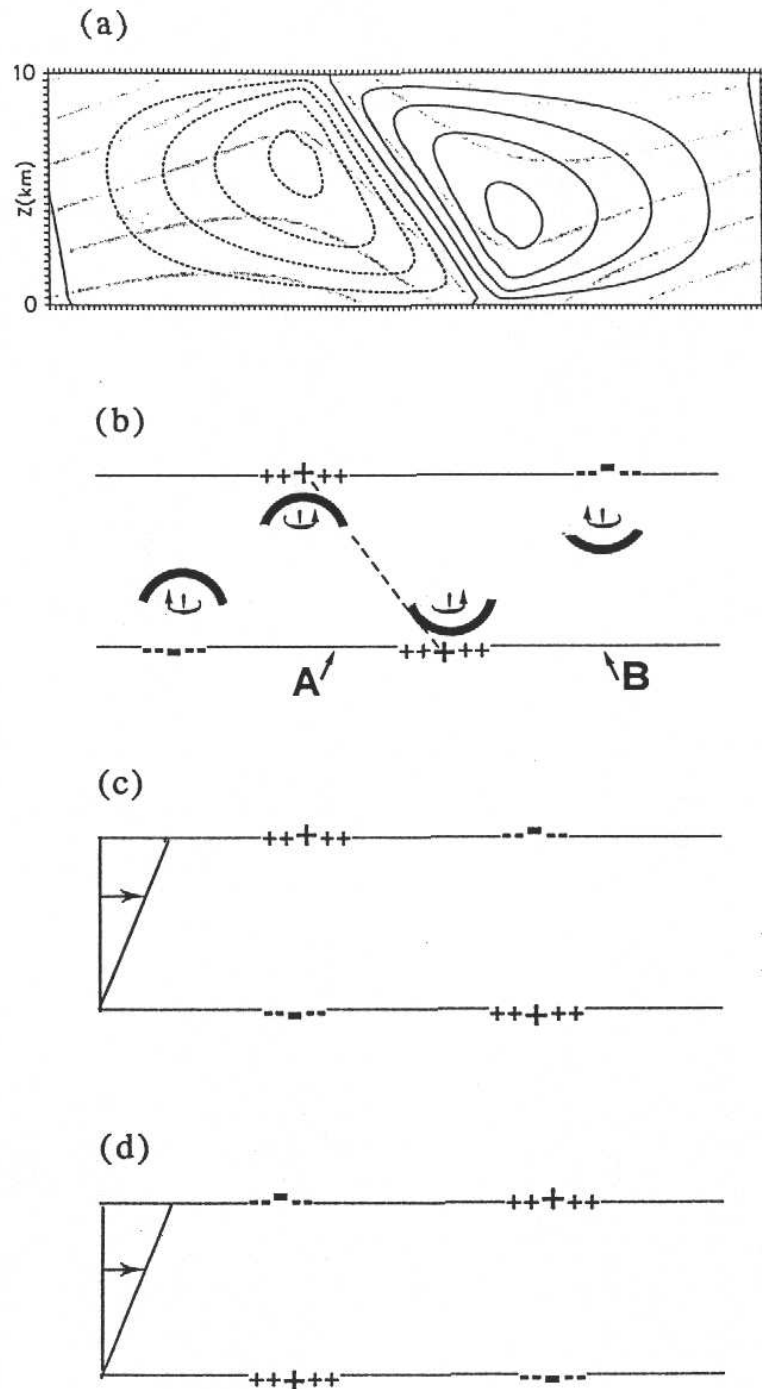


Figure 3.4: Features of a semi-geostrophic realization of horizontal shear-induced frontogenesis in a vertically bounded domain. The setting is that of the nonlinear normal mode for the two-dimensional Eady model. Panel (a) shows the isentropes (shaded) and the along-front velocity field (continuous lines) shortly before frontal collapse (From Snyder et al. 1993). Panel (b) is a schematic of the pseudo-PV anomalies on the bounding surfaces together with an indication of their near-field vorticity / circulation and isentropic displacement. Dashed line indicates the alignment of the pseudo-PV anomalies. Panels (c) and (d) depict two alternative configurations of initially localized PV distributions.

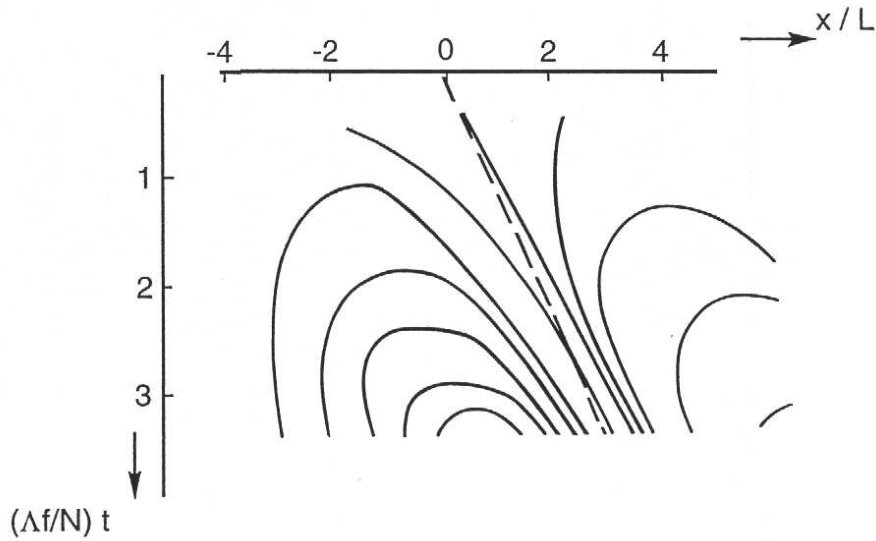


Figure 3.5: The quasi-geostrophic space-time evolution of the surface isentropes in response to a localised interior PV-anomaly initially implanted at $(x, z) = (0, h)$ in an uniform baroclinic shear within a semi-infinite domain. The anomaly has a δ -function structure in the vertical and a bell-shape, i.e. $[1 + (x/L)^2]^{-1}$, in the horizontal. The long-dashed line denotes the location of the centre of the PV anomaly at $z = h$ as it is advected with the background baroclinic flow field. To ensure quasi-monochromatic forcing the half width L and the height h have been set such that $L \sim 1.5(N/f)h$. [Note also that $\Lambda f/Nt = 2.5$ is order of 1 day, and that for this linear problem the constant increments of the isentropic isolines is arbitrary].

illustration consider an anomaly comprising a δ -function vertical structure located at a height h and with a bell-shape horizontal distribution, Surface waves generated with a wavenumber $k \sim (f/Nh)$ propagate with a phase-velocity $\sim \Lambda f/Nk$ that is comparable to that of the advecting velocity at level h , i.e. $U_{z=h} = \Lambda h$. Such waves will experience a quasi-monotonic forcing and can grow almost resonantly. Fig. 3.5 shows the space-time evolution of the surface potential temperature field in response to such a PV-anomaly.

3.4 Limits on the Frontogenesis

The foregoing theoretical examples illustrated the scale-collapse of a front in a finite time. This growth in the barocithicity might be curtailed by:- the reorientation or reduction in amplitude of the deformation associated with the large-scale field; unbalanced effects excluded from the semi-geostrophic system; three-dimensional effects; and diffusive effects.

A modification of the deformation field on the time-scale of frontal development is certainly possible since as noted earlier the frontogenesis time scale is linked to that of the evolution of the synoptic scale flow. Likewise for horizontal shear-induced frontogenesis the finite width of an ambient baroclinic zone will limit the surface thermal contrast that can evolve across the front.

From the standpoint of the limitations of the SG system itself, studies indicate that the two-dimensional semi-geostrophic flow developments discussed earlier remain valid until just prior to frontal collapse (e.g. Williams, 1967; Hoskins and Bretherton, 1972; Davies and Muller, 1984; Snyder et al. 1993; Nakamura, 1994), and even then only break down in a shallow narrow band. For example for the deformation-induced frontogenesis discussed earlier this band is of order 1 km wide and 30 m deep (Fig 3.6a).

One theoretical approach to the study of the post-collapse phase is to presume that the SG equations remain valid and to allow extrusions of the boundary pseudo-PV into the interior (e.g. Cullen and Purser, 1984; Koshyk and Cho, 1992). Such an extrusion forms a sloping frontal line of discontinuity comprising an interior S-function of potential vorticity (Fig. 3.6b). In this supra-balanced development the intrusion from the surface is accompanied by an upwelling of the low-level isentropes and hence in enhanced ascent ahead of the front.

More generally the development of spatially rich flow features in the transition toward a scale collapse can result in the forcing of unbalanced flow, an enhanced role for diffusive effects, and the development of balanced flow structures that are potentially unstable. Here we give consideration is given to each of these effects.

3.5 GENERATION OF UNBALANCED FLOW

The generation of unbalanced flow in the region of impending flow breakdown could both modify the in-situ balanced flow and possibly influence the far-field by the emission of inertia-buoyancy waves. Equilibration might prevail if the balanced flow-tendency for local scale-contraction was *either* countered by diffusive effects or matched by the adjustment of energy and momentum induced by the wave emission. The former possibility has a counterpart in the development of shock or bore-like phenomena, whilst the latter has a parallel with the turbulent generation of aerodynamic noise (Lighthill, 1952) and is also analogous to the breakdown of balanced flow over topography (Trüb and Davies, 1995).

For equilibration via wave emission an assessment or interpretation of the nature of wave-response can be sought by decomposing the flow into balanced and residual flow components and evaluating the space-time structure of the balanced-field's forcing of residual flow (Ley and Peltier, 1978; Snyder et al. 1993).

Explicit consideration of the dynamics of the breakdown using primitive equation numerical models requires very fine spatial and temporal resolution to accurately capture the nature of the ensuing motion without generating spurious buoyancy waves (see the discussions in Pecnick and Keyser, 1989; Volkert and Bishop, 1990; Snyder et al, 1993). The simulations of Snyder et al. (1993) show evidence of wave activity in the approach to breakdown, and indicate that in the post-collapse phase, when dissipative effects are strong, the waves become stationary relative to the front and modify the prefrontal ascent (Fig. 3.6c). An earlier suggestion (Orlanski and Ross, 1984) that the residual flow could induce a negative feedback upon the surface divergence and so curtail the frontogenesis has not received corroboration (see Levy and Bretherton, 1987; and Garner, 1989).

3.6 DIFFUSIVE EFFECTS

Diffusive effects can directly and significantly counter the scale contraction once the front attains a very fine spatial scale. In addition surface processes condition the potential vorticity in the planetary boundary layer and therefore air extruded into the interior will form PV-anomalies (Nakamura and Held, 1989; Cooper et al. 1992). Simulations of the two-dimensional Eady wave (Nakamura and Held, 1989; Nakamura, 1994) indicate an equilibration of the development as the PV anomalies from the upper (artificial) rigid boundary and the surface are vertically realigned by the background flow.

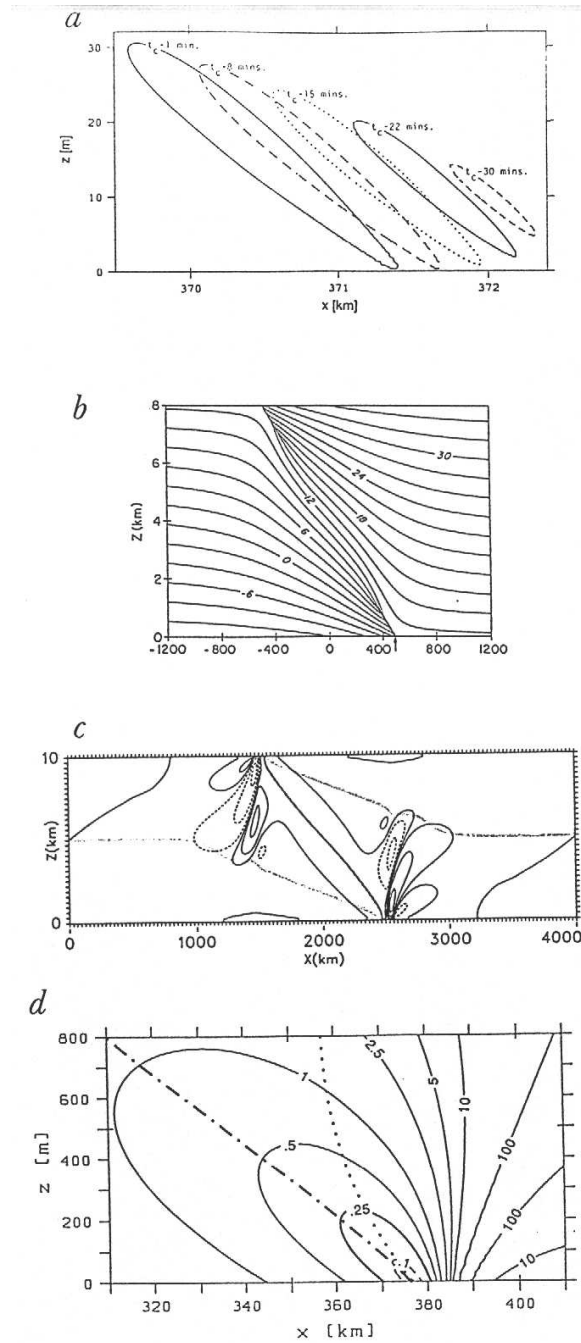


Figure 3.6: Illustrations of some features related to frontal scale-collapse. Panel (a): Error evolution of the SG set during the deformation-induced frontogenesis corresponding to Fig 3.2 (from Davies and Mller, 1988). The error is defined as the ratio of the neglected inertia terms to the Coriolis term in the across-front momentum equation. Isolines demark the shape of the $10 (df)^2$ error measure, and t_c refers to the time of the scale-collapse. (Spatial scale of the domain is $\sim 2.5 \text{ km} * 30 \text{ m}$). Panel (b): Isentropic distribution following an extrusion of the pseudo-PV anomalies of the bounding surfaces into the interior in the post-collapse phase (from Koshyk and Cho, 1992). Panel (c): Inertia-buoyancy waves emitted in a PE simulation at an advanced stage of the Eady two-dimensional setting of horizontal shear-induced frontogenesis (from Snyder et al. 1993). Shown is the non-balanced component of the vertical velocity field. Panel (d): The Ri distribution two hours prior to scale-collapse for the case of deformation-induced frontogenesis corresponding to Fig. 3.2 (from Mller, 1989).

3.7 UNSTABLE FLOW CONFIGURATIONS

An *instability* of the balanced flow in the approach to a scale-collapse would ensue if the evolving flow was unstable to unbalanced two-dimensional or (balanced or unbalanced) three-dimensional perturbations. To explore these possibilities consider the semi-geostrophic potential vorticity (q_{SG}),

$$q_{SG} = \left[(\zeta + f) \frac{\partial \theta}{\partial y} - \frac{\partial v}{\partial z} \frac{\partial \theta}{\partial x} + \frac{\partial u}{\partial z} \frac{\partial \theta}{\partial y} \right]$$

This can be rewritten, using the thermal wind relationship, in the form

$$\left(\frac{g}{\theta_0} \right) f q_{SG} = f^2 N^2 \left[1 + \left(\frac{\zeta}{f} \right) - Ri \right] \quad (3.18)$$

or equivalently,

$$\left(\frac{g}{\theta_0} \right) f q_{SG} = S^2 \left[1 + \left(\frac{\zeta}{f} \right) Ri - 1 \right] \quad (3.19)$$

where the Richardson Number (Ri) and the baroclinicity measure (S) are defined as

$$Ri = \frac{N^2}{\left(\frac{\partial u}{\partial z} \right)^2 + \left(\frac{\partial v}{\partial z} \right)^2}, \quad \text{and } S^2 = \left(\frac{g}{\theta_0} \right)^2 \left[\left(\frac{\partial \theta}{\partial x} \right)^2 + \left(\frac{\partial \theta}{\partial y} \right)^2 \right]$$

Note further that the potential vorticity of the ambient atmosphere is usually positive and is such that

$$\left(\frac{g}{\theta_0} \right) f q_{SG} \approx f^2 N^2 \quad \text{since typically both } (\zeta/f) \text{ and } Ri \ll 1 \quad (3.20)$$

Conservation of q_{SG} during the inviscid, dry frontogenesis discussed earlier implies that,

$$\left[\left(1 + \frac{\zeta}{f} \right) - Ri \right] > 0 \quad (3.21)$$

This inequality is also the necessary condition for stability to ageostrophic, two-dimensional (x, z) perturbations of the balanced flow if the latter is assumed to be time-independent.

Again note that an increase of ζ and S during frontogenesis induces a concomitant decrease in a fluid parcel's Richardson Number (see Eq. 3.19). It has been argued that domains characterized by $Ri < 1$ can sustain turbulence, whilst the criterion $Ri < 1/4$ is linked to the Kelvin-Helmholtz (K-H) type of instability - at least in flows that are less laterally structured than frontal zones. It follows from Eq. (3.19, 3.20) that the evolution of the Richardson Number in semi-geostrophic flow is prescribed by the relationship,

$$Ri \approx \frac{1 + \frac{(f^2 N^2)_{t=0}}{S^2}}{1 + \frac{\zeta}{f}},$$

and, when the baroclinicity S assumes large values characteristic of frontal zones, this reduces further to,

$$Ri \approx \frac{1}{1 + \frac{\zeta}{f}} \quad (3.22)$$

Thus the critical Richardson number ($Ri = 1/4$) is attained for vorticity values of $\zeta/f \sim 3$, and such values for the vorticity can develop significantly prior to frontal collapse. For

example Fig 3.6d shows the Richardson Number structure two hours before the scale collapse for the case of deformation-induced frontogenesis considered earlier. The $Ri < 1/4$ domain is $\sim 15 \text{ km} \times 250 \text{ m}$, and thus the onset and occurrence of a K-H instability could place a limit on the frontal width and baroclinicity. For this particular case the surface vorticity and baroclinicity are related and the presumed critical across-frontal length scale $(\Delta x)_{\text{crit}}$ is scaled by the relationship,

$$(\Delta x)_{\text{crit}} \sim \frac{1}{3} \left(\frac{g}{\theta_0} \right) \left[\left(\frac{\Delta\theta}{fN} \right) \right]_{t=0} \quad (3.23)$$

where $\Delta\theta$ and N represent respectively the initial values of the potential temperature difference across the broad frontal zone and the ambient stratification. A caveat to the foregoing discussion is that it remains to detect or explicitly model this small-scale three-dimensional process within a zone undergoing strong frontogenesis.

Note also that a banded interior PV anomaly formed by extrusion of anomalous positive potential vorticity from the planetary boundary layer will form a maximum of PV in the interior and such a distribution is a potential seat for a three-dimensional balanced-flow instability. Diabatic effects (see next sub-section) can also give rise to interior PV extremae.

3.8 Cloud-Diabatic and Surface Friction Effects

The nature of convection triggered within a low-level frontal convergence zone will be highly dependent upon the vertical thermodynamic structure. An organized ensemble of such convective elements could feedback directly or indirectly upon the front. The feedback will be indirect if the organization takes the form of one or more squall lines propagating ahead of the front and thereby conditioning the pre-frontal environment. It can be direct if there is a space and time-scale matching of the ensemble and the front - c.f. an elongated non-transient meso-scale cloud band aligned almost parallel to and propagating with the surface front. Such interaction could be sustained and compatible with balanced-flow dynamics, c.f. the postulate of quasi-balance for some mesoscale convective systems (Raymond, 1992; Davis and Weisman, 1993; Parker and Thorpe, 1995).

It is therefore instructive to examine the form of the convection-front interaction(s) from a balanced-flow and PV-perspective. The initial location and width of the convective region within an evolving front would be linked to the low-level convergence pattern and the domain demarked by fluid parcels first attaining their lifting condensation level. In general the latter will be significantly less than the width of the ascending region itself. This decreased width coupled with an effective decrease in the vertical stratification within the convective region will favour (Eq. 2.7) a narrower and stronger region of ascent. Within the region of organized convection the diabatic heating will yield a PV-tendency that is positive beneath the level of maximum heating and negative above (see Eq. 2.5a). The realization of a positive low-level PV anomaly would be accompanied at lower levels by (i) cyclonic vorticity and (ii) an elevation of the isentropes. In general signal (i) will be favoured by a deep narrow diabatic domain (c.f. deep penetrative convection) and signal (ii) by a shallower broader distribution (c.f. layered stratocumulus).

The foregoing features can influence the frontogenesis in several ways. For the case of deformation-induced frontogenesis, prior to the onset of convection, the low-level ascent and surface convergence is centred at the vorticity maximum ahead of the surface front (Eqs. 3.4a, b). Thus signal (i) will increase the rate of vorticity production (Eq. 2.6) and signal (ii) will promote additional ascent. The latter can lead to a positive feedback with the additional low-level ascent enhancing the moisture flux convergence into the cloud region. The isentropic and perturbed PV fields (Fig. 3.7) derived from a SG simulation of deformation-induced frontogenesis in the presence of parameterized stratiform clouds (Chan and Cho, 1991) shows the surface

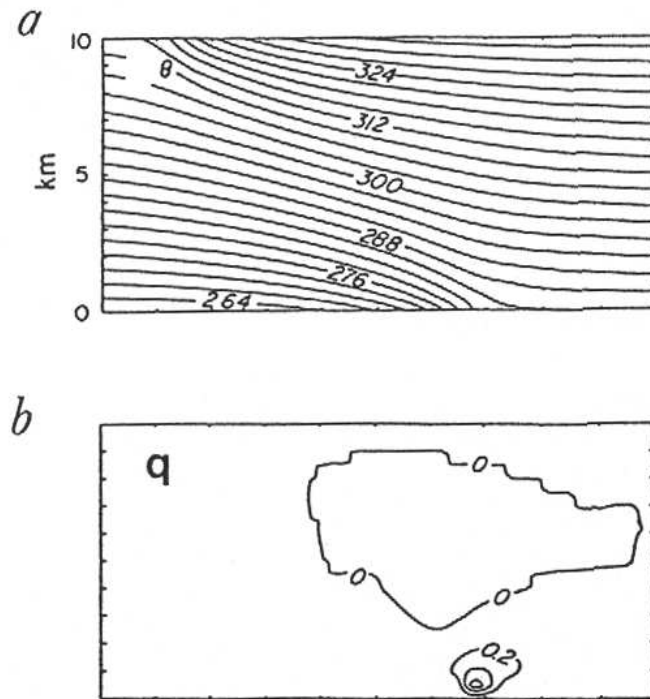


Figure 3.7: An SG simulation of deformation-induced frontogenesis with a parameterization of stratiform clouds. The upper and lower panels show respectively the potential temperature field and the perturbed PV field. (From Chan and Cho, 1991).

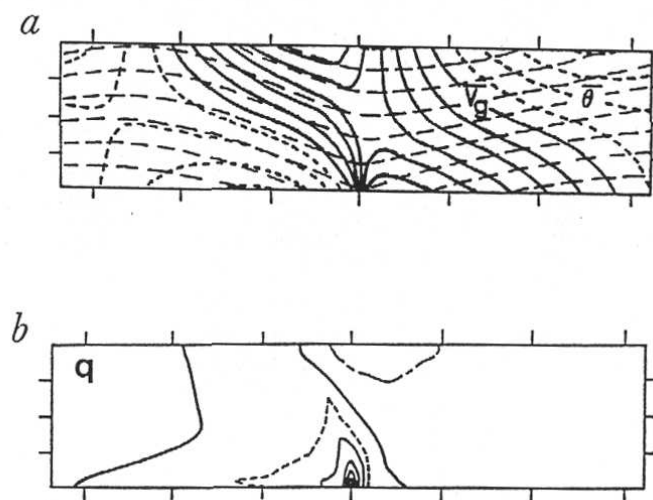


Figure 3.8: An SG simulation of the Eady setting with a parameterization of slant-wise convection. Panel (a) shows the potential temperature and along-front velocity fields and panel (b) the perturbed PV field. (From Joly and Thorpe, 1989).

front and the low-level PV anomaly suitably located to sustain and to be enhanced by these effects.

For the case of horizontal shear-induced frontogenesis prior to the onset of convection, the low-level convergence is located in the warm sector ahead of the surface front. In addition to the forementioned interactions there are now effects linked to the ambient along-front baroclinicity. To illustrate this consider the influence and evolution of a diabatically-induced low-level PV anomaly. The accompanying cyclonic vorticity will augment the surface frontogenesis. There is also the possibility (see Section 3c) that as this anomaly is advected eastward by the ambient flow it will remain suitably phased relative to the propagating anomaly in the surface baroclinicity, and thereby instigate and be sustained by further diabatic heating. Fig. 3.8 is an example of the structure that evolves within a SG model of horizontal shear-induced frontogenesis that includes a parameterization of slant-wise convection.

In general numerical modelling studies of the deformation case (Malt and Bannon, 1984; Thorpe and Emanuel, 1985; Chan and Cho, 1991) and the horizontal shear case (Emanuel et.al. 1987; Knight and Hobbs, 1988; Joly and Thorpe, 1989; Whitaker and Davis, 1994) do show narrower and more intense updrafts but the scale, structure and location(s) of the updrafts are sensitively dependent upon the cloud parameterization schemes.

It was noted earlier that diffusive effects within the boundary layer can counter frontal scale-contraction and lead to interior PV-anomalies. In addition surface frictional effects can modify the rate and direction of frontal propagation within the boundary layer and the strength and width of the low-level convergence zone (Blumen, 1990). Detailed consideration of these effects for a range of boundary layer structures has yet to be undertaken. Simulations of the archetypal frontogenesis configurations undertaken with numerical models that include a representation of the turbulent boundary layer do produce a narrower and more intense updraft (Keyser and Anthes, 1982, 1986; Reeder and Smith, 1986) and significant interior PV-anomalies (Cooper et al. 1992). An important caveat to these studies is our limited understanding of the turbulent PBL response when forced by highly structured and rapidly varying mesoscale free-atmosphere flow.

Chapter 4

Frontogenesis in an idealised three-dimensional setting

Fronts and cyclones develop concurrently in the atmosphere and are interrelated both in terms of their origin and dynamics. This co-development is studied here in the classical idealized setting of baroclinic instability.

Consider the extended Eady model comprising an incompressible flow of uniform potential vorticity sandwiched between two rigid horizontal boundaries on an f -plane. The basic state is assigned the form of a two-dimensional jet-like baroclinic flow that is characteristic of the zonally-averaged mid-latitude troposphere. As before the dynamics of perturbations to this state can be viewed in terms of upper- and lower-boundary pseudo-PV waves propagating on the laterally-confined baroclinicity at these surfaces. In contrast to the two-dimensional setting the Q -vector frontogenetic forcing field now develops internally during the flow evolution, and moreover the vorticity field can rotate the evolving surface frontal zone into, or out of, alignment with the dilatation axis of the prevailing deformation field (*c.f.* Eqs. 2.1, 2.3).

4.1 Evolution within a Symmetric Basic State

In Fig. 4.1 an example is shown of the finite-amplitude structure of the most unstable normal-mode of a symmetric jet-like flow in the SG, adiabatic, and inviscid limit. To the south of the evolving surface cyclone the presence of a distinct thermal gradient and significant wind shift and vorticity signatures are all indicative of strong frontogenesis. This cold front's thermal gradient is weaker in the vicinity of the cyclone itself, but to the south-west it extends around the base of the anticyclone. There is also some evidence of a weak, short warm front that bends outward and eastward from the cyclone centre.

At the surface the cold front's resemblance to the counterpart two-dimensional fronts (see Chapter 3.1, 3.2) is striking. It has narrow co-located bands of vorticity and convergence ahead of the baroclinic zone, indications of strong deformation field with its dilatation axis aligned along the front, and active frontogenesis along a substantial portion of the frontal band. For the bent-back warm front it is the lack of correspondence with the archetypes of Chapter 3 that is striking. Far from the cyclone the dominant feature is the broad and strong signature in the $(\nabla_h \theta)$ field, whereas the surface baroclinicity and vorticity signatures only attain significant amplitude in the vicinity of the cyclone. A tentative inference, that is explored later, is that this warm front is an intrinsically three-dimensional feature.

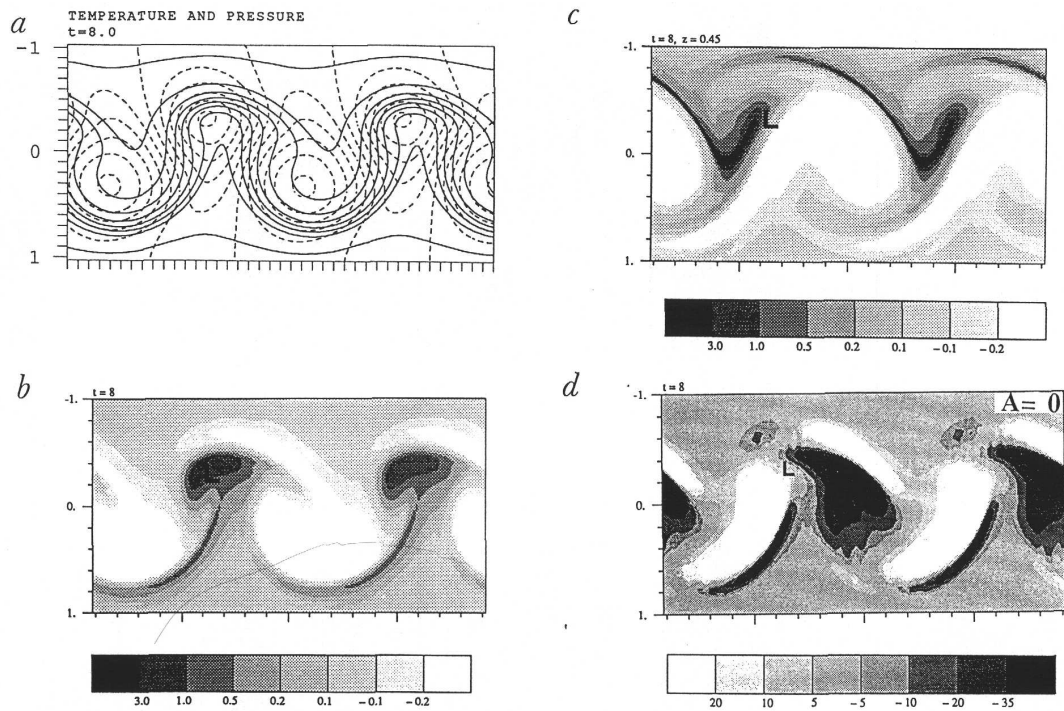


Figure 4.1: Features of nonlinear normal-mode development of a symmetric jet-like baroclinic basic state as captured by the SG system (from Davies et al. 1991). Panel (a) shows the surface distribution of the isentropes (solid lines) and streamfunction (dashed lines). Panels (b) and (c) show respectively the surface and upper-boundary vorticity patterns, and panel (d) the surface quasi-geostrophic ($\nabla_h \mathbf{Q}$ field.)

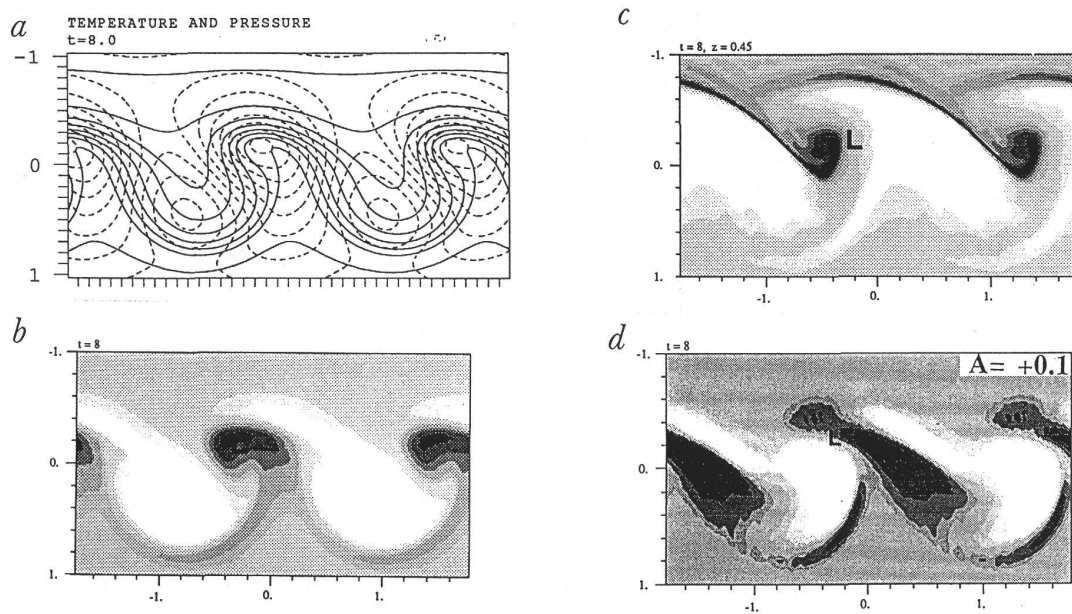


Figure 4.2: As for Fig. 4.1 but for the "cyclonic" case with positive shear superimposed upon the basic state (from Davies et al. 1991).

4.2 Evolution for an Asymmetric Basic State

The foregoing frontal features reflect a symmetry constraint imposed upon the flow development by the combination of the SG system on an f-plane and the symmetric basic state (Davies et al., 1991). This symmetry does not in general prevail for : more complex systems (the primitive equations); different geometrical settings (the β -effect or spherical geometry); or asymmetric basic states (e.g. the presence of lateral barotropic shear or internal PV gradients).

In essence the symmetry state of the SG system can be viewed as a bifurcation point in parameter space with the nature of the ensuing fronts differing radically in response to the sign of the asymmetry. The *PE system on an f-plane* favours the earlier, stronger, and spatially more extended development of the warm front (see e.g. Takayabu, 1986; Keyser et al. 1989; Polavarapu and Peltier, 1990; Snyder et al. 1991; Tremblay, 1992; Lalaurette et al. 1994; Rotunno et al. 1994). Contrariwise the *PE system in spherical geometry* tends to induce stronger and more elongated cold frontal features (see e.g. Thorncroft and Hoskins, 1990; Hines and Mechoso, 1991; Whitaker and Snyder, 1992). These dichotomous responses can be replicated in the *SG f-plane system* by the simple expedient of adding to the symmetric basic state a weak uniform positive (negative) barotropic shear to favour surface warm (cold) frontogenesis with upper-level vortex-like (band-like) pseudo-PV features (Davies et al. 1991).

There are indications that lateral shear is indeed the dominant symmetry-breaking factor. For example the starkly differentiated response to lateral shear in the SG f-plane system is paralleled in the PE f-plane system (Fchimann and Wcrnli, private communication), and are integral to the two paradigms of baroclinic-wave life-cycle behaviour identified in simulations with the PE spherical geometry system (see Thorncroft et al., 1993; and Simmons - this volume). In light of the foregoing we focus here on the two forms of response engendered by the addition of weak barotropic shear.

Figs. 4.2 and 4.3 illustrate the characteristics of the two forms in the f-plane SG setting. For the "cyclonic" case of positive shear (Fig. 4.2) the thermal pattern of the cold front is severely disrupted to the immediate south-east of the cyclone (c.f. the phenomenon of frontal fracture), and there is evidence of a bent-back warm frontal feature. The frontal palette takes on a distinctive λ -shape - particularly in the $(\nabla_h \cdot Q)$ field, and aloft at the lid a vorticity band extends north-westward from a vortex structure that is located almost above the surface cyclone. In the "anticyclonic" case of negative lateral shear (Fig. 4.3) the patterns of vorticity and $(\nabla_h \cdot Q)$ directly link the cyclone and cold front, whereas the warm front is weaker. At the lid the southward protrusion of cold air is now bordered by frontal / vorticity features and the leading edge is aligned parallel to, but displaced NW of, the surface cold front.

The ambient lateral shear, which in both cases amplifies considerably during the flow development, clearly exerts a profound influence upon the strength and structure, and the distinctiveness of the ensuing fronts. *In relation to the strength and structure* note that positive (negative) lateral shear can be decomposed (Fig. 4.4a) into a positive (negative) rotation plus a deformation field with a dilatation axis aligned NW-SE (NE- SW). Thus in the positive (negative) lateral shear case the incipient warm (cold) front is favourably orientated to benefit from the additional deformation. This is consistent with the lateral shears contribution to the frontogenesis index (Eq. 2.2). The shear's contribution to the vertical velocity, via the $(\nabla_h \cdot Q)$ field (Eqs. 2.7), can be inferred qualitatively from the schematic of the shear-related Q-vectors of Fig. 4.4b. They suggest that for the cyclonic shear case frontogenesis is extended south-eastward at the warm front, and curtailed in the vicinity of the cyclone at the cold front. The reverse applies for the case of anticyclonic shear.

In relation to the distinction between frontal types a notable feature is the disparity of the lateral-shear induced changes to the $(\nabla_h \cdot Q)$ and vorticity patterns at both the warm and cold front (Figs. 4.2, 4.3). Yet these two parameters are strongly coupled via Eqs. 2.7, 2.8. To

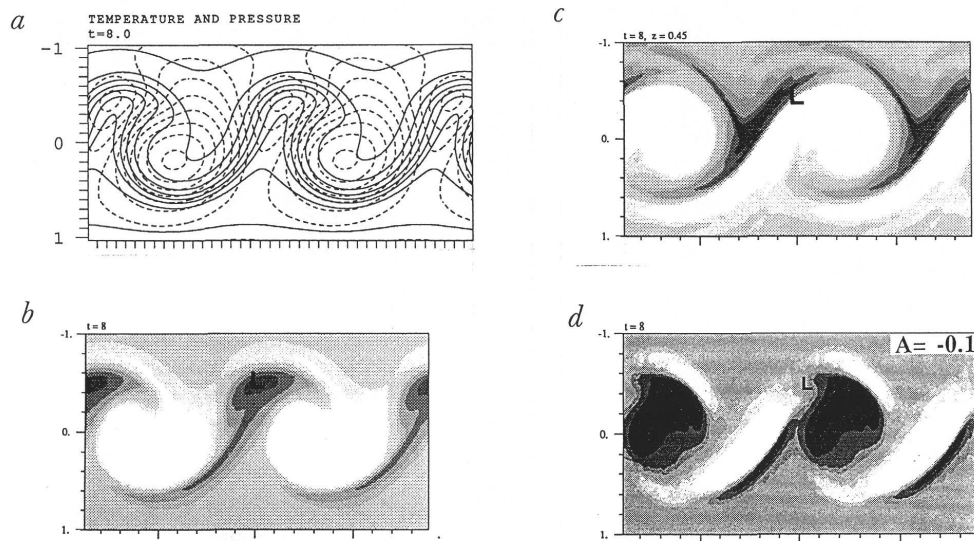


Figure 4.3: As for Fig. 4.1 but for the "anticyclonic" case with negative shear superimposed upon the basic state (from Davies et al. 1991).

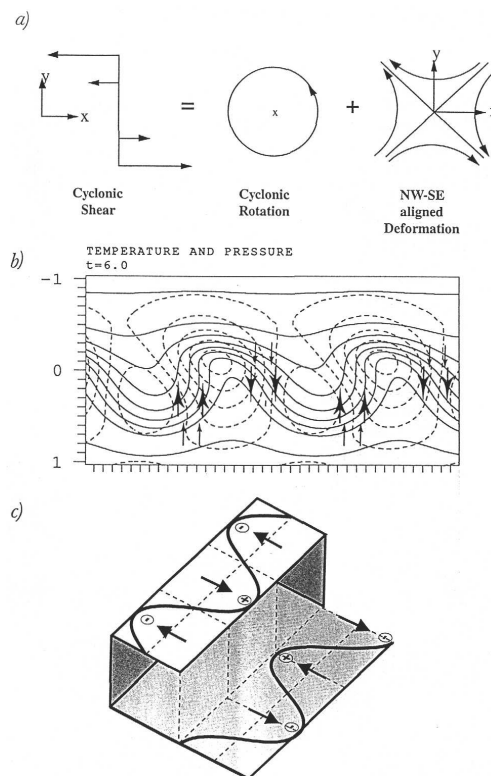


Figure 4.4: Illustration of features influencing the nature of frontal development. Panel (a): the decomposition of a positive lateral shear into its invariant components - i.e. a rotation and a NW-SE aligned deformation field. Panel (b): the dominant Q -vector signal attributable to positive ambient lateral shear (indicated by the arrows) within an incipient baroclinic wave development. Panel (c) the location and displacements of the upper and lower-boundary pseudo-PV anomalies for a basic state with the upper baroclinic zone located northward of the surface zone. (Note the approach of the upper and lower level positive pseudo-PV-anomalies).

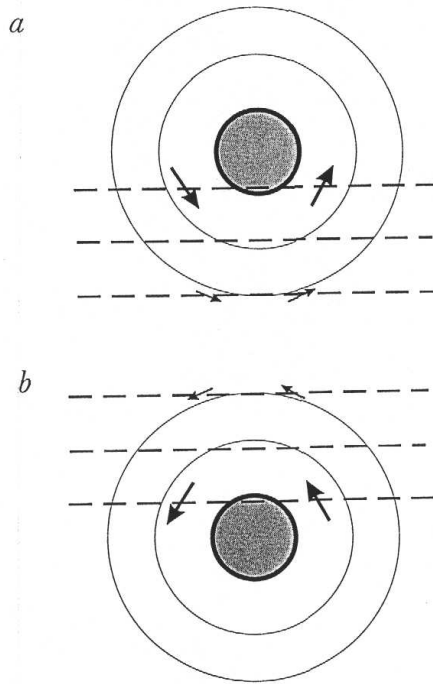


Figure 4.5: Schematics of features associated with a positive PV-anomaly (shaded feature) located (a) poleward and (b) equatorward of a low-level baroclinic zone (dashed lines denoting the surface isentropes). The arrows signify the contribution of the PV-anomaly to the flow within the baroclinic zone.

interpret this difference note that, in the presence of strong surface convergence and associated vorticity production, a weak (strong) relative airflow along the front will result in the vorticity being realized in-situ (downstream). Now consider the contributions to this low-level relative air-flow from a PV perspective, i.e. in terms of the contributions attributable to the thermal anomalies on the two bounding surfaces. For the case of positive lateral-shear the contributions of the surface and upper-level thermal anomalies counter one another significantly at the cold front, whereas the upper-level contribution is comparatively weak at the warm front. This is consistent with the appearance (non- appearance) of an in-situ band of vorticity along the cold (warm) front. (The location of the upper and lower level anomalies can be inferred qualitatively from the upper-level vorticity signatures in Fig. 4.2). This dependence of the nature of the frontogenesis upon the relative alignment of the upper and lower level pseudo-PV anomalies resembles and extends the dynamical distinction drawn earlier between two-dimensional cold and warm fronts.

At the forefront of the preceding discussion has been the diagnostic influence of the ambient lateral shear. The dynamics of the shear's development itself is more subtle. The shear renders the basic jet flow asymmetric and this induces a lateral shift in the relative locations of the upper and lower boundary thermal waves. During the nonlinear development this lateral shift for the cyclonic case (say) results in the positive pseudo-PV anomalies on the upper and lower boundaries approaching, interacting and almost overlying one another, whilst the negative anomalies move apart. (The initial approach is schematized in Fig. 4.4c and the result of the subsequent evolution is evident in Fig. 4.2). This relative movement of the anomalies can in turn account for the amplification of the shear during the evolution.

4.3 Influence of Some Other Factors

The frontal patterns in Fig. 4.2 and 4.3 resemble many of the structural features of observed atmospheric fronts, but diabatic and boundary layer processes can again modify the nature of the frontogenesis. For the simulated cold fronts their structural and dynamical resemblance to the two-dimensional counterparts suggests that their diabatic modification might also be somewhat similar. For the warm fronts their intrinsically three-dimensional structure with bands of strong front-relative flow and low-level convergence suggests that their dynamics might be sensitive to frictional and diabatic effects. These inferences are supported by numerical simulations performed with PE models. For instance the inclusion of a bulk-aerodynamic representation of the surface drag (Hines and Mechoso, 1993) reduces the strength of the front-relative flow in the warm-frontal region and decreases that front's length. Likewise the inclusion of a simple convective parameterization scheme (Whitaker and Davis, 1994) yields low-level PV bands in the frontal convergence zones, and the subsequent advection of the potential vorticity at low-level along the bent-back portion of the warm front contributes directly to a more rapid and intense cyclogenesis.

The shear-related cyclonic and anticyclonic paradigms of development (Sections 4.1 and 4.2) might also be triggered by other physical variations that induce an asymmetry of the basic-state jet flow. Possible examples are anomalous shifts in SST patterns, e.g. a lateral shift of the lower boundary baroclinic zone relative to the upper zone or the presence of a finer-scaled warm band embedded within the surface zone. In the latter case numerical simulations indicate that the nature of the response is sensitive to the warm band's location with elements of the cyclonic paradigm resulting if the band is near the centre of the surface zone.

4.4 Comments on Upper-Level Fronts

In this study the focus throughout has been on surface frontogenesis. However distinctive front-like features also develop at the tropopause and are generally associated with V-shaped intrusions of stratospheric air down to tropospheric levels. (See Shapiro and Keyser (1990) for a recent overview.)

The theoretical examination of upper-level frontal features has paralleled that for surface fronts. Studies include idealized models of two-dimensional deformation-induced frontogenesis ranging from a simple two PV-layer representation of the troposphere-stratosphere interface (Hoskins, 1971; Hoskins and Brethenon, 1972) to a continuous PV representation (Moore, 1993; Saute, 1993). Likewise there have been detailed studies of the front-like upper-level features that develop within three-dimensional baroclinic waves growing on a jet-like basic state (e.g. Hines and Mechoso, 1991; Thorncroft et al. 1993; Bush and Peltier, 1994; Rotunno et al. 1994). From an interpretative standpoint it is germane to record that the starkly different upper-level patterns (Figs. 4.2 and 4.3) that evolve in a simple flow setting (f-plane, rigid lid) bear a marked resemblance to the patterns that evolve in a more general setting (spherical geometry, tropopause structure) and that were termed paradigmatic by Thorncroft et al. (1993).

Here we comment briefly upon tropopause-level versus surface frontogenesis, and confine our remarks primarily to PV-related aspects. At the surface a frontal development usually signifies the dynamical juxtaposition of air masses with distinctively different spatial origin and thermal characteristics. It is therefore appropriate to devise a dynamical index for frontogenesis in terms of the evolution of the surface baroclinicity (c.f. Eqs. 2.1-2.4). In contrast astride the tropopause there are pre-existing air masses with starkly different characteristics, and thus formulating an index for upper-level frontogenesis is more problematic. For example consider the traditional indices based upon potential temperature (Eqs. 2.1-2.2). In the free atmosphere these indices include the effect of tilting due to differential vertical advection, and their simple reduced

forms, valid on a flat surface (Eqs. 2.3, 2.4), are inapplicable. Moreover within a direct frontal circulation the tilting can substantially offset the in-situ effects of deformation and/or horizontal shear, and thereby render the diagnosis of frontogenesis a subtle assessment of counteracting effects (see e.g. Keyser and Shapiro, 1986; Hines and Mechoso, 1991; Shapiro and Keyser, 1990; Rotunno et al. 1994).

From a potential vorticity perspective the free-atmosphere analogue of the baroclinicity at the surface is the PV gradient on a θ -surface. Likewise an analogue of potential temperature frontogenesis at the surface would be the sharpening of an interior PV gradient on a θ -surface. Moreover it is at the mid-latitude tropopause-break that this PV-gradient is maximum, and indeed Reed and Danielsen (1960) identified an upper-level front as a quasi-discontinuity of potential vorticity on a θ -surface. It follows that the free-atmosphere dynamical counterpart of the traditional indices for surface frontogenesis (i.e. Eqs. 2.2, 2.4) are,

$$\left(\frac{D}{Dt}\right)_{\theta} \frac{1}{2}(\Delta_{\theta}q)^2 = -(\Delta_{\theta}q)^2 \left(\frac{\partial v}{\partial n}\right), \quad (4.1)$$

$$\left(\frac{D}{Dt}\right)_{\theta} (\Delta_{\theta}q) = -|\Delta_{\theta}q| \left(\mathbf{k} \times \left(\frac{\partial v}{\partial n}\right)\right), \quad (4.2)$$

where q is the potential vorticity, and the θ subscript refers to derivatives along a θ -surface.

These PV-related measures circumvent consideration of the forementioned counteracting effects, and enable a qualitative appraisal of the frontogenesis to be made by inspection of the potential vorticity and wind field distributions on a tropopause-transcending isentropic chart (c.f. discussion following Eq. 2.4). In addition many of the deductions and interpretations advanced above to account for the characteristics / types of surface fronts can be reformulated in terms of PV patterns on an isentropic chart and applied to upper-level fronts. (As an aside we note that these frontogenesis measures can not be applied to the rudimentary but standard two PV-layer representation of the tropopause that are used for model studies of frontogenesis / tropopause folding. This is either a deficiency of the measures outlined here or an indication of the inappropriateness of the model as an idealization of free-atmosphere frontogenesis).

Chapter 5

The Frontal Palette and Cyclogenesis Types

Consideration is now given to the nature of the frontogenesis and the frontal palette associated with presumed paradigmatic precursor patterns for cyclogenesis. Classifications of surface cyclogenesis exist that are based upon a synthesis of synoptic (e.g. Petterssen and Smeybe, 1971), satellite (e.g. Smigielski and Ellrod, 1985; Weldon and Holmes, 1994), or composite (Young, 1994) data. These schemes identify two broad classes of surface development, and here we comment briefly upon the nature of the frontal palette that can accompany these classes.

5.1 Upper-Level Induced Development

The first type is the response to the passage of an upper-level trough (or equivalently a positive PV-anomaly) toward a surface baroclinic zone, and there are further refinements to distinguish between a NW-SE and NE-SW alignment of the upper-level anomaly. This first type can be viewed as an initial-value counterpart of baroclinic instability with a finite-amplitude initial perturbation, and the refined criteria related to the incipient structures of the cyclonic and anticyclonic paradigms discussed in Sections (4a, b).

A theoretically-based approach to the study of this type is to implant a finite-amplitude upper-level anomaly upon a jet-like baroclinic basic state, and to examine the resulting flow evolution (e.g. Takayabu, 1991; Schär and Wernli, 1993). A key initial feature is the anomaly's deformation of the surface baroclinic zone to form a dipole of negative-positive thermal anomalies aligned along the zone. For a prescribed basic state the nature of the subsequent development will be a function of the location, strength and structure of the PV-anomaly.

Conformity with observations would place the anomaly over or to the cold side of the surface baroclinic zone. For the first setting the pure kinematic distortion of the baroclinic zone (c.f. Keyser et al. 1988) will favour cold and warm frontogenesis respectively to the SW and NE. The second displaced setting introduces two further effects. Firstly the across-front component of the anomaly's contribution to the surface flow field favours frontogenesis (frontolysis) to the SW(SE) on the incipient cold (warm) front as can be inferred from Fig. 4.5a. Secondly the along-front component contribution counters that attributable to the surface baroclinic zone and thereby helps promote the in-situ realization of the vorticity.

The subsequent evolution is influenced by a range of effects including the dispersion of the initial surface dipole along the low-level zone of enhanced baroclinicity, the analogue process on the upper-level FV-gradient, and the distortion and advection of the original PV-anomaly by the ambient flow. Growth of the initial surface perturbations will again be enhanced in this case if they remain suitably phased with the translating upper-level anomaly (see Fig. 3.5).

5.2 PV-Band Instability

The second type is the evolution of wave-like disturbances on a mature frontal zone. In recent years this type has been linked to the instability of the low-level pre-frontal band of diabatically-produced potential vorticity produced during of moist frontogenesis. Growth to finite-amplitude of unstable waves on this band can lead to the band's breaks up into a train of isolated segments (Schär and Davies, 1990; Malardel et al. 1993). Each segment now constitutes a low-level PV-anomaly located on the warm side of the surface baroclinic zone (see Fig. 4.5b). In this case the simple qualitative considerations of the previous sub-section lead to the reversed inferences of frontogenetic (frontolytic) tendencies to the NE (NW) on the warm (cold) front, and these inferences are sustained by the results of numerical simulations (Schur and Davies, 1990; Malardel et al. 1993).

5.3 Other Configurations

In general the two key cyclogenetic features of the ambient atmosphere - the surface baroclinic zone and the zone of strong PV gradient on troposphere-transcending potential temperature surfaces - are not co-aligned. In such situations the predilection for a surface disturbance to propagate along the surface baroclinic zone can result in a change in that low-level system's ambient environment and also in its location relative to a pre-existing upper-level anomaly. Shapiro (this volume) draws attention to such an effect. For example consider a shallow system propagating north-eastward from the sub-tropics along a surface baroclinic zone aligned with the North-Atlantic SST pattern. It would in effect move away from the influence of the strong tropopause-level PV gradient of the sub-tropical jet stream and come closer to the meandering and anomaly rich features of the mid-latitude jet. In this process the surface disturbance would experience a marked change in its ambient cross-front shear and, in light of the foregoing, be susceptible to a modification of its frontal palette.

Chapter 6

Further Remarks

Research on fronts and frontogenesis has both forecast-orientated and explanatory-related objectives. It is instructive to view the development and current trends in the theoretical study of frontogenesis through the lens of these objectives. In the development of the research the contributions of the Bergen School were seminal. Their method of synoptic analysis delivered a crisp, physically-based, portrayal of the frontal palette of mid-latitude weather systems on surface charts. It provided meteorologist with a readily assimilated tool capable of representing key frontal features, pinpointing probable areas of precipitation, and tracing the day-to-day evolution of frontal weather patterns.

It prompted primarily forecast-orientated studies. The comparative success and utility of the method long discouraged the development and use of alternative analysis techniques. On the one hand the basis for the analysis method was accepted and attempts made to elaborate the procedure (see e.g Chromow, 1940, Willett, 1944), whereas on the other hand the forecaster often pragmatically tailored the results of applying the technique to mask rather than highlight incongruities with the prevailing weather features (Sutcliffe, 1952). Neither approach was undergirded by a significant theoretical base, and Sawyer (1964) remonstrated (and demonstrated) that the increase in available observations, technological advances and better understanding of atmospheric dynamics did make "it possible to display succinctly on one chart several features of atmospheric structure which are not adequately described by conventional frontal analysis". This refrain has been repeated sporadically thereafter. For example Mass (1992), assessing the issue from a synoptician's standpoint, provides a detailed critique of the currently perceived limitations of the original frontal analysis technique.

Bergerons exploration of frontogenesis (Bergeron, 1928) was predominantly explanatory in character, as have been the subsequent theoretical studies surveyed in the present study. Seminal to advance in this field was the formulation of the semi-geostrophic (SG) system of equations (Eliassen, 1959,1962; Hoskins, 1971,1975; Hoskins and Bretherton, 1972). The foundational studies (Chapter 3) based principally upon the SG system isolated the key mechanisms for inducing frontogenesis, illustrated the central role of the geostrophically-forced ageostrophic circulation in generating rapid frontogenesis. established a dynamical basis for the distinction between cold and warm fronts, pinpointed the processes limiting frontal scale-contraction, and helped clarify the role of frictional and diabatic effects. Studies of frontogenesis in the idealized setting of growing baroclinic waves (Chapter 4) indicated that the range of simulated patterns include several realistic features, and that the realized frontal palette is sensitive to the geometry, the nature of the flow system, and the ambient shear. These studies provide a platform for understanding the frontal palette that accompanies observed events of cyclogenesis (Chapter 5).

In relation to forecast-orientated objectives the theoretical studies of frontogenesis have served for example: to demonstrate the value and limitations of the primitive equations; to indicate the two-way inter-scale linkages between fronts, cyclones and the larger-scale flow; to

underline the significance of these linkages to the occurrence and nature of frontogenetic events; and to provide physically-meaningful diagnostic tools for analyzing the observed phenomena.

Future theoretical studies can help in the development insightful way(s) of examining both analysis and forecast fields. This challenge is heightened by the ability to view synoptic and frontal development with time loop displays from one (or more) three- dimensional perspectives. Future theoretical (and observational) research areas can be highlighted by the limitations and capabilities of the current operational forecasting suites. For example rapid fronto- and cyclogenesis remains a major forecasting problem. Also the ability to perform ensemble forecasts with even high resolution meso-scale limited- area models raises the intriguing issue of the degree of deterministic space-time predictability of fronts. These possible future research directions are linked to both forecast and explanatory science, and as such follow the pathway exemplified by the Bergen School.

REFERENCES

- Bannon, P.R., 1984 : Effects of stratification on surface frontogenesis: warm and cold fronts. *J. Atmos. Sci.*, 41, 2021-2026. fronts. *J. Atmos. Sci.*, 41, 2021-2026.
- Bergeron, T., 1928: Ober die dreidimensional verknüpfende Wetteranalyse. *Geophys. Pub./* 6(6), 111pp.
- Bishop, C.H., 1993: On the behaviour of baroclinic waves undergoing horizontal deformation . I: The "RT" phase diagram. *Quart. J. Roy. Met. Soc.* 119, 221-240.
- Blumen, W., 1980: A comparison between the Hoskins-Bretherton model of frontogenesis and the analysis of an intense surface frontal zone. *J. Atmos. Sci.*, 37, 64-77. , 64-77.
- Blumen, W., 1981: The geostrophic coordinate transformation. *J. Atmos. Sci.*, 38, 1100 -1105.
- Blumen, W., 1990: A semi-geostrophic Eady-wave frontal model incorporating momentum diffusion: Part I: Model and solutions. *J. Atmos. Sci.*, 47, 2890-2902.
- Browning, K.A., 1990: Organization of clouds and precipitation in extratropical cyclones. In "Extratropical Cyclones: The Erik Palmeri Memorial Volume", Amer. Meteor. Soc. Boston. 265 pp.
- Chan, D. and H-R. Cho, 1991: The dynamics of moist frontogenesis in a semi- geostrophic model. *Atmos-Ocean*, 29, 85-101.
- Chromow, S.P., 1940: *Einführung in die synoptische Wetteranalyse*, Springer, Vienna, 532pp.
- Cooper, I.M., Thorpe, A.J. and C.H. Bishop, 1992: The role of diffusive effects on potential vorticity in fronts. *Quart. J. Roy. Met. Soc.*, 118, 629-647.
- Cullen, M.J.P. and R.J. Purser., 1984: An extended Lagrangian theory of semi- geostrophic frontogenesis, *J. Atmos. Sci.*, 41, 1477-1497.
- Davies, H.C. and J.C. Müller, 1988. Detailed description of deformation-induced semi-geostrophic frontogenesis. *Quart. J. Roy. Met. Soc.*, 114, 1201-1219.
- Davies, H.C., Sehär, Ch., and H. Wernli, 1991: The palette of fronts and cyclones within a baroclinic wave-development. *J. Atmos. Sci.*, 48, 1666-1689.
- Davies, H.C. and C.H. Bishop, 1994: Eady edge waves and rapid development. *J. Atmos. Sci.*, 51, 1930-1946.
- Davis, C.A., and M.L. Weisman, 1994: Balanced dynamics of mesoscale vortices produced in simulated convective systems. *J. Atmos. Sci.*, 51, 2005-2030.
- Eliassen, A., 1959: On the formation of fronts in the atmosphere. *The Rossby Memorial Volume . Rockefeller Institute Press, New York, 277-287.*
- Eliassen, A., 1962: On the vertical circulation in frontal zones. *Geophys. Pub./* 24, 147- 160.
- Eliassen, A., 1990: Transverse circulations in frontal zones. In "Extratropical Cyclones The Erik Palmfn Memorial Volume", Amer. Meteor. Soc. Boston. 265 pp.
- Emanuel, K.A., Fantini, M. and A.J. Thorpe, 1987: Baroclinic instability in an environment of small stability to slantwise moist convection. Part I: Two dimensional models. *J. Atmos. Sci.*, 44, 1559-1573.
- Gall, R., Williams, R.T. and T.L. Clark, 1988: Gravity waves generated during frontogenesis. *J. Atmos. Sci.*, 46, 2205-2219.
- Garner, S.T., 1989: Fully Lagrangian numerical solutions of unbalanced frontogenesis and frontal collapse. *J. Atmos. Sci.*, 46, 717-739.
- Hines, K.M. and C.R. Mechoso, 1991: Frontogenesis processes in the middle and upper troposphere. *Mon.Wea.Rev.*, 119, 1225-1241.
- , and - , 1993: Influence of surface drag on the evolution of fronts. *Mon.Wea. Rev.*, 121, 1152-1175.
- Hoskins, B.J., 1971: Atmospheric frontogenesis models: Some solutions. *Quart. J. Roy. Met. Soc.* 97, 139-153.

Hoskins, B.J., 1975: The geostrophic momentum approximation and the semigeostrophic equations. *J. Atmos. Sci.*, 32, 233-242.

Hoskins, B.J., 1982: The mathematical theory of frontogenesis. *Ann. Rev. Fluid Mech.* 14, 131-151.

Hoskins, B.J. and F.P. Bretherton, 1972: Atmospheric frontogenesis models: Mathematical formulation and solutions. *J. Atmos. Sci.*, 29, 11-37.

Hoskins, B.J., Draghici, I. and H.C. Davies, 1978: A new look at the co-equation. *Quart. J. Roy. Met. Soc.*, 104, 31-38.

Hoskins, B.J. and N.V. West, 1979: Baroclinic waves and frontogenesis. Part II: Uniform potential vorticity jet flows. *J. Atmos. Sci.*, 36, 1663-1680.

Hoskins, B.J. and W.A. Heckley, 1981: Cold and warm fronts in baroclinic waves. *Quart. J. Roy. Met. Soc.*, 107, 79-90.

Hoskins, B.J., Neto, E.C. and H: R. Cho, 1984: The formation of multiple fronts. *Quart. J. Roy. Met. Soc.*, 110, 881-896.

Hoskins, B.J., McIntyre, M.E. and A.W. Robertson, 1985. On the use and significance of isentropic potential vorticity maps. *Quart. J. Roy. Met. Soc.*, 111, 877-946.

Joly, A. and A.J. Thorpe, 1989: Warm and occluded fronts in two-dimensional moist baroclinic instability. *Quart. J. Roy. Met. Soc.*, 115, 513-534.

Keyser, D. and R.A. Anthes, 1982: The influence of planetary boundary layer physics on frontal structure in the Hoskins-Bretherton horizontal shear model. *JAtmos.Sci.*, 39, 1783-1802.

Keyser, D. and R.A. Anthes, 1986: Comments on "Frontogenesis in a moist semigeostrophic model". *JAtmos.Sci.*, 43, 1051-1054.

Keyser, D. and M.A. Shapiro, 1986: A review of the structure and dynamics of upper-level frontal zones. *Mon. Wea. Rev.*, 114, 452-499.

Keyser, D. and M.J. Pecnick, 1987: The effect of along-front temperature variation in a two-dimensional primitive equation model of surface frontogenesis. *J. Atmos. Sci.*, 44, 577-604.

Keyser, D., Reeder, M.J., and R.J. Reed, 1988: A generalization of Petterssen's frontogenesis function and its relation to the forcing of vertical motion. *Mon.Wea. Rev.*, 116, 762-780.

Keyser, D., Schmidt, B.D., and D.G. Duffy, 1989: A technique for representing three-dimensional vertical circulations in baroclinic disturbances. *Mon.Wea. Rev.*, 117, 2463-2494.

Knight, D.J. and P.V. Hobbs, 1988. The mesoscale and microscale structure and organization of clouds and precipitation in midlatitude cyclones. Part XV: A numerical study of frontogenesis and cold-frontal rainbands. *J. Atmos. Sci.*, 45, 915-930.

Koshyk, J.N. and H-R. Cho, 1992: Dynamics of a mature front in a uniform potential vorticity semi-geostrophic model. *J. Atmos. Sci.*, 49, 497-510.

Lalaurette, F., Fischer, C., and J.-P. Cammas, 1994: Location and interaction of upper- and lower-tropospheric adiabatic frontogenesis. *Mon.Wea. Rev.*, 122, 2004-2021.

Levy, G. and C.S. Bretherton, 1987: On a theory of evolution of surface cold fronts. *J Atmos. Sci.*, 44, 3413-3418.

Lighthill, M.J., 1952: On sound generated aerodynamically. I General Theory. *Prot. Roy. Soc. A*, 211, 564-587.

Malardel, S., Joly, A., Courbet, F. and Ph. Courtier, 1993: Nonlinear evolution of ordinary frontal waves induced by low level potential vorticity anomalies. *Quart. J. Roy. Met. Soc.*, 119, 681-714.

Mak, M. and P.R. Bannon, 1984: Frontogenesis in a moist semi-geostrophic model. *J. Atmos. Sci.*, 41, 3485-3500.

Mass, C.F., 1991: Synoptic analysis: Time for a reassessment. *Bull. Amer. Met. Soc.*, 72, 348-363.

Moore, G.W.K., 1993: The development of tropopause folds in two-dimensional models of

- frontogenesis. *J. Atmos. Sci.*, 50, 2321-2334.
- Müller, J., 1989: Semi-geostrophische Entwicklung von Fronten and Störungen in der unteren Atmosphäre. PhD Dissertation No. 8878, ETH Zurich, 179pp.
- Müller, J., Davies, H.C. and Ch. Scher, 1989: An unsung mechanism for development. *J. Atmos. Sci.*, 46, 3666-3672.
- Nakamura, N., 1994: Nonlinear equilibration of two-dimensional Eady waves: Simulations with viscous geostrophic momentum equations. *J. Atmos. Sci.*, 51, 1023-1035.
- Nakamura, N. and I.M. Held, 1989: Nonlinear equilibration of two-dimensional Eady waves. *J. Atmos. Sci.*, 46, 3055-3064.
- Ogura, Y. and D. Portis, 1982: Structure of the cold front observed in SESAME-AVE III and its comparison with the Hoskins-Bretherton frontogenesis model. *J. Atmos. Sci.*, 39, 2773-2792.
- Orlanski, I and B.B. Ross, 1984: The evolution of an observed cold front. Part II: Mesoscale dynamics. *J. Atmos. Sci.*, 41, 1669-1703.
- Ostdiek, V. and W. Blumen, 1995: Deformation frontogenesis: Observations and theory. *J. Atmos. Sci.*, 39, 1783-1801.
- Parker, D.J. and A.J. Thorpe, 1995: Conditional convective heating in a baroclinic atmosphere: a model of convective frontogenesis. *J. Atmos. Sci.*, 52, 1699-1711.
- Pecnick, M.J., and D. Keyser, 1989: The effect of spatial resolution on the simulation of upper-tropospheric frontogenesis using a sigma-coordinate primitive equation model. *Meteor. Atmos. Phys.*, 40, 137-149.
- Petterssen, S., 1936: A contribution to the theory of frontogenesis. *Geophys. Publ.*, 11, 1-27.
- Petterssen, S., and S.J. Smeybe, 1971: On the development of extratropical cyclones. *Quart. J. Roy. Met. Soc.*, 97, 457-482.
- Polavarapu, S.M. and W.R. Peltier, 1990. The structure and nonlinear evolution of synoptic scale cyclones: life cycle simulations with a cloud scale model. *J. Atmos. Sci.*, 47, 2645-2672.
- Raymond, D.J., 1992: Nonlinear balance and potential-vorticity thinking at large Rossby number. *Quart. J. Roy. Met. Soc.*, 118, 987-1105.
- Reed, R.J. and E.P. Danielsen, 1960: Fronts in the vicinity of the tropopause. *Arch. Met. Geophys. Biold. A*, 11, 1-17.
- Reeder, M.J., and R.K. Smith, 1986: A comparison between frontogenesis in the two-dimensional Eady model of baroclinic instability and summertime cold fronts in the Australian region. *Quart. J. Roy. Met. Soc.*, 112, 293-313.
- Rotunno, R., Skamarock, W.C., and C. Snyder, 1994: An analysis of frontogenesis in numerical simulations of baroclinic waves. *J. Atmos. Sci.*, 51, 3373-3398.
- Saute, M., 1993: The influence of tropospheric static stability on upper-level frontogenesis. *Tellus*, 45A, 159-167.
- Sawyer, J.S., 1956: The vertical circulation at meteorological fronts and its relation to frontogenesis. *Proc. Roy. Soc. A*, 234, 346-362.
- Sawyer, J.S., 1964: Meteorological analysis - a challenge for the future. *Quart. J. Roy. Met. Soc.*, 90, 227-247.
- Schär, Ch. and H.C. Davies, 1990: An instability of mature cold fronts. *J. Atmos. Sci.*, 47, 929-950.
- Schär, Ch. and B. Wemli, 1993: Structure and evolution of an isolated semi-geostrophic cyclone. *Quart. J. Roy. Met. Soc.*, 119, 57-90.
- Shapiro, M.A. and D. Keyser, 1990: On the structure and dynamics of fronts, jet streams and the tropopause. In "Extratropical Cyclones: The Erik Palmer: Memorial Volume", Amer. Meteor. Soc. Boston. 265 pp.
- Smigielski, F.J. and G.P. Ellrod, 1985: Surface cyclogenesis as indicated by satellite imagery. NOAA (F.M.NESDIS 9), Washington D.C. 30pp.

- Snyder, C., Skamarock, W. C., and R. Rotunno, 1991: A comparison of primitive- equation and semi-geostrophic simulations of baroclinic waves. *J. Atmos. Sci.*, 48, 2179-2194.
- Snyder, C., Skamarock, W.C. and R. Rotunno, 1993: Frontal dynamics near and following frontal collapse. *J. Atmos. Sci.*, 50, 3194-3211.
- Stone, P.H., 1966. Frontogenesis by horizontal wind deformation fields. *J. Atmos. Sci.*, 23, 455-465.
- Sutcliffe, R.C., 1952: Principles of synoptic weather forecasting. *Quart. J. Roy. Met. Soc.*, 78, 291-320.
- Takayabu, I., 1986: Roles of the horizontal advection on the formation of surface fronts and on occlusion of a cyclone developing in the baroclinic westerly jet. *J. Met. Soc. Japan* , 64, 329-345. 38 Takayabu, I., 1991: "Coupling development": An efficient mechanism for the development of extratropical cyclones *J. Met. Soc. Japan* , 69, 609-628.
- Thorneroft, C. and B.J. Hoskins, 1990: Frontal Cyclogenesis. *J. Atmos. Sci.*, 47, 2317-2336.
- Thomcroft, C., Hoskins, B.J., and M.E. McIntyre, 1993: Two paradigms of baroclinic- wave life-cycle behaviour. *Quart. J. Roy. Met. Soc.*, 119, 17-56.
- Thorpe, A. J. and K.A. Emanuel, 1985: Frontogenesis in the presence of small stability to slantwise convection. *J. Atmos. Sci.*, 42, 1809-1824.
- Tremblay, A., 1992: Structure and development of mesoscale baroclinic waves in a nonhydrostatic numerical model. *Mon. Wea. Rev.*, 120, 463-481.
- Trüb, J. and H.C. Davies, 1995: Flow over a mesoscale ridge: pathways to regime transition. *Tellus*, 47A, 502-524.
- Volkert, H. and C.H. Bishop, 1990: The semi-geostrophic Eady problem as a testbed for numerical simulations of frontogenesis. *Tellus*, 42A, 202-207
- Weldon, R.B. and S.J. Holmes, 1991: Water vapour imagery interpretation and applications to weather analysis and forecasting. NQAA Technical Report NESDIS 57, Washington, D.C., 213pp.
- Whitaker, J.S. and C. Snyder, 1992 : The effects of spherical geometry on the evolution of baroclinic waves. *J. Atmos. Sci.*, 50, 597-612.
- Whitaker, J.S. and Davis, C.A., 1994: Cyclogenesis in a saturated environment. *J. Atmos. Sci.*, 51, 889-907.
- Willett, H.C., 1944: *Descriptive Meteorology*, Academic Press, New York, pp.
- Williams, R.T., 1967: Atmospheric frontogenesis: A numerical experiment. *J. Atmos. Sci.*, 24, 627-641.
- Williams, R.T., 1968: A note on quasi-geostrophic frontogenesis. *J. Atmos. Sci.*, 25, 1157-1159.
- Young, M.Y., 1994: A classification scheme for cyclone life cycles: Applications in analysis and short-period forecasting. In "The Life Cycles of Extratropical Cyclones". *Proc. Intl. Symposium, Bergen*. Vol. III, 380-385. 39